



January 2018

# Synthesis And Characterization Of Novel Bioplastics By Innovative 3d Printing Approaches

Kathryn Marie Hall

Follow this and additional works at: <https://commons.und.edu/theses>

---

## Recommended Citation

Hall, Kathryn Marie, "Synthesis And Characterization Of Novel Bioplastics By Innovative 3d Printing Approaches" (2018). *Theses and Dissertations*. 2408.

<https://commons.und.edu/theses/2408>

This Thesis is brought to you for free and open access by the Theses, Dissertations, and Senior Projects at UND Scholarly Commons. It has been accepted for inclusion in Theses and Dissertations by an authorized administrator of UND Scholarly Commons. For more information, please contact [zeinebyousif@library.und.edu](mailto:zeinebyousif@library.und.edu).

SYNTHESIS AND CHARACTERIZATION OF NOVEL BIOPLASTICS BY INNOVATIVE  
3D PRINTING APPROACHES

by

Kathryn Marie Hall  
Bachelor of Science, University of North Dakota, 2016

A Thesis

Submitted to the Graduate Faculty

of the

University of North Dakota

In partial fulfillment of the requirements

for the degree of


Master of Science

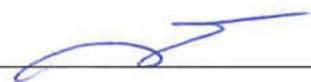
Grand Forks, North Dakota

December  
2018

Copyright 2018 Kathryn Hall


This thesis, submitted by Kathryn Hall in partial fulfillment of the requirements for the Degree of Master of Science in Chemical Engineering from the University of North Dakota, has been read by the Faculty Advisory Committee under whom the work has been done and is hereby approved.


  
\_\_\_\_\_  
Dr. Surojit Gupta

  
\_\_\_\_\_  
Dr. Yun Ji

  
\_\_\_\_\_  
Dr. Frank Bowman

This thesis is being submitted by the appointed advisory committee as having met all of the requirements of the School of Graduate Studies at the University of North Dakota and is hereby approved.

  
\_\_\_\_\_  
Grant McGimpsey  
Dean of the School of Graduate Studies

  
\_\_\_\_\_  
Date

## PERMISSION

Title            Synthesis and Characterization of Novel Bioplastics by Smart 3D Printing Approaches  
Department    Chemical Engineering  
Degree         Master of Science

In presenting this thesis in partial fulfillment of the requirements for a graduate degree from the University of North Dakota, I agree that the library of this University shall make it freely available for inspection. I further agree that permission for extensive copying for scholarly purposes may be granted by the professor who supervised my thesis work or, in his absence, by the Chairperson of the department or the dean of the School of Graduate Studies. It is understood that any copying or publication or other use of this thesis or part thereof for financial gain shall not be allowed without my written permission. It is also understood that due recognition shall be given to me and to the University of North Dakota in any scholarly use which may be made of any material in my thesis.

Kathryn Hall

December 6, 2018

## TABLE OF CONTENTS

LIST OF FIGURES.....	vii
LIST OF TABLES.....	ix
ACKNOWLEDGEMENTS.....	x
ABSTRACT.....	xii
CHAPTER	
I. INTRODUCTION	
1.1 Biopolymers.....	1
1.1.1 Lignin.....	2
1.1.2 Polylactic Acid.....	3
1.2 MAX Phases.....	5
1.3 MAB Phases.....	8
1.4 Additive Manufacturing.....	9
II. LIGNIN/PLA AM COMPOSITES	
2.1 Introduction.....	12
2.2 Experimental.....	13
2.3 Results and Discussion.....	16
2.4 Conclusions.....	17
III. MAX/MAB POL AM COMPOSITES	
3.1 Introduction.....	19
3.2 Experimental.....	19
3.3 Results and Discussion.....	28
3.4 Conclusions.....	42
IV. CONCLUSIONS AND FUTURE WORK	
4.1 Future Studies on Lignin- PLA Composites.....	43
4.2 Experimental.....	43
4.3 Concluding Remarks.....	44

APPENDIX

REFERENCES..... 45

## LIST OF FIGURES

Figure	Page
1.1 The MAX phases consist of an early transition metal M (red) in the periodic table, an element from the A group, usually IIIA and IVA (dark blue), and a third element, X, which is either nitrogen or carbon (black), in the composition $M_{n+1}AX_n$ , where n is 1, 2 or 3. ....	6
1.2 Crystal Structure of the 211, 312, and 413 MAX phases .....	6
2.1 Schematics of, (a) a 3D printer printing PLA-50 wt% Lignin composition, and (b) a PLA-50 wt% Lignin 3D printed sample. ....	15
2.2 Tensile Stress vs Displacement of 3D Printed and Solvent-Cast PLA-Lignin Composites. ....	17
3.1 Schematics of the extruder used for designing filaments for 3D printing. ....	22
3.2 Afinia H400 3D printer.....	25
3.3 Sample dimensions for 3D printed testing coupons (a) tensile test coupon (dimensions in mm) (b) cylindrical test coupon.....	25
3.4 SEM micrographs of extruded filaments of, (a) PLA in SE, and BSE images of, (b) BSE of (a), (c) PLA-1wt% MoAlB, (d) PLA-5wt% MoAlB, (e) PLA-1wt% $Ti_3SiC_2$ , (f) PLA-5wt% $Ti_3SiC_2$ , (g) PLA-1wt% $Ti_3AlC_2$ , (h) PLA-5wt% $Ti_3AlC_2$ , (i) PLA-1wt% $Cr_2AlC$ , and (j) PLA-5wt% $Cr_2AlC$ .....	30
3.5 SEM micrographs of 3-D printed, (a) PLA in SE, and BSE images of, (b) BSE of (a), (c) PLA-1wt% MoAlB, (d) PLA-5wt% MoAlB, (e) PLA-1wt% $Ti_3SiC_2$ , (f) PLA-5wt% $Ti_3SiC_2$ , (g) PLA-1wt% $Ti_3AlC_2$ , (h) PLA-5wt% $Ti_3AlC_2$ , (i) PLA-1wt% $Cr_2AlC$ , and (j) PLA-5wt% $Cr_2AlC$ .....	32
3.6 Plot of, (a) porosity, and (b) hardness versus MAX or MAB content in the PLA matrix. ....	34
3.7 DSC analysis of, (a) PLA, (b) PLA-1 wt% MoAlB, (c) PLA-5 wt% MoAlB, (d) PLA-1wt% $Ti_3SiC_2$ , (e) PLA-5 wt% $Ti_3SiC_2$ , (f) PLA-1 wt% $Ti_3AlC_2$ ,	



(g) PLA-5 wt% $Ti_3AlC_2$ , (h) PLA-1 wt% $Cr_2AlC$ , and (i) PLA-5 wt% $Cr_2AlC$ . .....	35
3.8 Plot of tensile stress versus displacement of 3D printed PLA. ....	35
3.9 Plot of tensile stress versus displacement of, (a) PLA-MoAlB, (b) PLA- $Ti_3SiC_2$ , (c) PLA- $Ti_3AlC_2$ , and (d) PLA- $Cr_2AlC$ . ....	36
3.10 Plot of tensile strength versus MAX or MoAlB additions in the PLA matrix. ....	38
3.11 Plot of, (a) friction coefficient, and (b) WR versus MAX or MAB additions in PLA matrix. ....	39
3.12 SEM micrographs of, (a) PLA in SE, (b) BSE image of the Stainless steel surface, (c) PLA-5wt% $Cr_2AlC$ in BSE, (d) higher magnification of PLA-5wt% $Cr_2AlC$ in BSE, (e) Stainless steel surface in BSE, and (f) BSE of the region marked in (e) after tribological testing. ....	40
3.13 Wettability profile of, (a) PLA, (b) PLA-1wt% $Ti_3SiC_2$ , (c) PLA-5wt% $Ti_3SiC_2$ , (d) PLA-1wt%MoAlB, (e) PLA-5 wt% MoAlB, (f) PLA-1wt% $Ti_3AlC_2$ , (g) PLA-5wt% $Ti_3AlC_2$ , (h) PLA-1 wt% $Cr_2AlC$ , and (i) PLA-5 wt% $Cr_2AlC$ . ....	41
3.14 Plot of Contact angle as a function of MAX or MoAlB content.....	41

## LIST OF TABLES

Table	Page
1.1 A list of MAX phases known to date, in both bulk and thin film form.....	7
2.1 Summary of the tensile strengths of 3D printed PLA-lignin composites.....	17
3.1 Materials extruded along with their composition and nomenclature used. ....	20
3.2 Optimized settings for various filament compositions.....	24

## **ACKNOWLEDGMENTS**

I wish to acknowledge and express my sincere appreciation to the following individuals that have supported me, not only during the course of this project, but throughout my Master's degree.

First, I would like to express my gratitude to my advisors Dr. Surojit Gupta and Dr. Yun Ji for their support and guidance throughout the duration of my Master's program.

I would also like to thank the members of our advanced materials research group for their assistance with materials testing, teamwork and thought-provoking conversations.

And finally, I would like to thank all of my family and friends, especially my parents Craig and Kellie. You have all encouraged me to reach my goals and have helped me to succeed in this endeavor.

To my kookums,  
for always encouraging me.

## ABSTRACT

This work describes the synthesis and characterization of novel bioplastic composites by using novel additive manufacturing (AM) approaches. As a background, global plastic consumption has become a problem with the accumulation of plastics in landfills and the ocean. Recently, bioplastics have emerged as a viable option to petrochemicals. Currently, there are some issues like biodegradability, property optimization with bioplastics etc. In this thesis, novel methods and engineering of composition of bioplastics are being reported. In Chapter II, the addition of lignin to the PLA polymer matrix by using solvent mixing will be reported. During this study, liquid ink mixture was successfully printed by using modified “drop on demand” material extrusion approach. Uniaxial tensile tests showed that 3D printed lignin-PLA composites have similar tensile strength as solvent cast samples. In Chapter III, the MAX/MAB phases were mixed with PLA matrix by using dry ball milling. The mixed compositions were then melt processed into filaments by using extruders. The filaments of composites of MAX/MAB phase with PLA were then printed by Fused Deposition Modeling (FDM). Detailed microstructure and characterization of 3D printed compositions will be reported. In this thesis,  $\text{Ti}_3\text{SiC}_2$ ,  $\text{Ti}_3\text{AlC}_2$ ,  $\text{Cr}_2\text{AlC}$ , and  $\text{MoAlB}$  were studied.

# CHAPTER I

## INTRODUCTION

### 1.1 Biopolymers

Biopolymers are polymers that are derived from natural resources and crude oil. There are multiple ways that they can be categorized, two of the most common being by, (a) source, and (b) by base unit or repeated unit in the polymer chain [1-4]. In this study, a classification by source is being reported for comparison with our work. When categorized by source, there are four categories, namely: (A) direct extraction from the natural raw materials such as biomass. Some examples of biopolymers extracted are polysaccharides like starch and cellulose; proteins like gelatin, casein, and silk; and marine prokaryotes. (B) Production from bio-derived monomers via chemical synthesis such as lactic acid from biomass to produce polylactic acid (PLA). (C) Production of synthetic biopolymers by microorganisms or fermentation by genetically modified bacteria, for examples, polyhydroxyalkanoates (PHA), polyhydroxybutyrate (PHB), polyhydroxyvalerate (PHV), bacterial cellulose, xanthan, and pullan. (D) Production from crude oil by conventional and chemical methods, for example, aliphatic and aromatic polyesters, polyvinyl alcohol (PVA), and modified polyolefins. [2, 3]

Biopolymers have several important characteristics that make them an attractive alternative to fossil-fuel derived plastics. They are derived from a variety renewable resources, making them a sustainable material. They can replace conventional plastics in many single-use applications, such as plastic grocery bags, plastic cups, diapers, food containers, etc. They can be partially or fully biodegradable, which helps to decrease the amount of plastic accumulating in landfills

worldwide. They also have much less of an environmental impact than fossil-fuel derived plastics because the crops that they are derived from absorb CO<sub>2</sub> to grow. [4]

### 1.1.1 Lignin

Lignocellulose, or plant matter, is a copiously available variety of biomass. Lignocellulose consists mainly of lignin and the polysaccharides cellulose and hemicellulose. The polysaccharides make up about two-thirds of the biomass and can be used to produce ethanol, which can be used as a biofuel. [5, 6] Lignin makes up about 20-35% of dry lignocellulose weight, depending on the source of the biomass. [7]

Lignin is the second most abundant natural polymer, behind cellulose. It is a mixture of complex polymeric compounds and is concentrated in the cell walls of wood, making up 25-35 percent of the weight of softwoods and 20-25 percent of hardwoods. [7] Lignin is an aromatic compound that has a recalcitrant nature due to characteristics such as its cross-linked structure and composition. The properties of the lignin particulates such as chemical structure, molecular weight distribution, and the degree of crosslinking, are affected by lignin isolation methods. This leads to non-uniform and nonstandard quality lignin making it difficult to use. [8]

Lignin, a byproduct from the paper and pulping industry, has the potential to be used as an environmentally friendly filler in the plastics industry [9, 10]. However, cost-effective, reliable methods for the conversion and application of lignin are technically challenging due to the recalcitrant nature of lignin [10]. There are several advantages of using lignin as an additive in a polymer matrix. Some of the advantages are improving toughness, acting as a free radical trap, improving flame resistance, modifying the biodegradability, improving photo resistance and thermal stability, expanding fatigue lifetime, and contributing to the green engineering of materials [10].

Even though there are many advantages of using lignin as an environmentally friendly filler, raw unprocessed lignin poses several challenges. Some of these challenges are, (a) chemically heterogeneous nature of lignin, (b) incompatibility between lignin and polymer matrix due to chemical incompatibility, (c) difficulty in melt processing, and (d) deleterious effect of lignin on the mechanical properties of lignin [11].

Several methods are being explored to work around the challenges that arise when working with lignin. These methods seek to deconstruct the lignin matrix to utilize it more effectively. There are both chemical and biological pathways for modifying the lignin matrix. Some researchers are modifying their lignin by functionalizing the OH groups in the lignin polymer matrix to make them more compatible with various polymers matrices. Modification methods include esterification reactions, acetylation reactions, and silanization reactions [10, 12-14]. Others are degrading the lignin matrix via biological and thermochemical processes to make use of the lower molecular weight molecules obtained from depolymerization to generate value-added products [7, 15]. Some are also finding innovative ways to incorporate lignin into more valuable products, such as thermoplastics without modifying the lignin matrix. [16, 17].

### 1.1.2 Polylactic Acid

Polylactic acid or PLA is a biodegradable thermoplastic polymer. It is derived from the monomer lactic acid. Lactic acid can be produced by bacterial fermentation of cellulose or chemical synthesis from acetaldehyde. Fermentation is the more favorable production method due to limitations of chemical synthesis of lactic acid. Limitations of chemical synthesis methods include a dependence on a byproduct of another process, their inability to produce the L-lactic acid monomer exclusively and high manufacturing costs. One of the main sources of cellulose used in



the production of PLA is corn starch and is the exclusive raw material for the company NatureWorks, the largest manufacturer of PLA in the US. [3, 18, 19]

PLA has many commercial applications especially in single use items such as food containers, cold drink cups, blister packaging, cutlery, plates, outdoor novelties, packaging applications, grocery bags, diapers, etc. [3] It can also have applications in the medical field as it is able to degrade into non-toxic lactic acid. The medical applications of PLA are in medical implants such as screws, rods, pins, and mesh since they can completely break down in the human body in 6 months to 2 years and eliminate needing an additional removal by surgery. [18]

Since PLA is a biodegradable plastic, it has a major advantage over traditional plastics. In the right conditions, it can biodegrade in less than a month's time as compared to traditional plastics which take several hundreds of years to biodegrade in landfills. PLA is very recyclable since it is a thermoplastic. This means that previously used PLA can be melted and remolded to a new shape. In addition, the process to manufacture PLA is much more environmentally friendly than traditional plastics. PLA production emits less greenhouse gases and has a much less energy intensive process than conventional plastic production. It requires 25-55% less energy to produce than traditional plastics and can even be lowered in the future. [20] Since carbon dioxide is absorbed during the growing process of the cellulose, the net greenhouse gas emission for PLA production can even be considered negative. [18] There are several other advantages of PLA which include:

- Excellent optical properties and high tensile strength [20]
- Ability to recycle back to lactic acid by hydrolysis or alcoholysis
- Capability of producing hybrid paper-plastic packaging that is compostable
- Reduction of landfill volumes

- Improvement of the agricultural economy
- Ability to tailor physical properties through material modifications
- Classified as generally recognized as safe (GRAS) by the United States Food and Drug Administration (FDA) and is safe for all food packaging applications [3]

PLA has several advantageous qualities, but there are some drawbacks of using it as well. Some issues with PLA include low deformation at break and low heat resistance but with high modulus. [21]. It is also considered inferior to polyethylene terephthalate (PET) for long-term food storage applications due to permeability issues which result in faster food spoilage. [18]

Recently, many researchers have attempted to alter the brittle nature of PLA by reinforcing the polymer with various fibers. It has been shown that the addition of fibers to the polymer matrix improved the mechanical properties in some cases. For instance, Sujaritjun et. al. [22] reported improved tensile strength with the addition of bamboo fibers and coconut fibers. Similarly, Tian et al. [23] reported a 25% higher bending strength of PLA composites reinforced with carbon fiber. However, Scaffaro et. al [24] reported a decrease in both tensile and flexural strength with increased addition of *Posidonia Oceanica*, a Mediterranean Sea seagrass.

## 1.2 MAX Phases

MAX phases are a family of layered ternary carbides and nitrides with the chemical formula  $M_{n+1}AX_n$ , where  $n= 1, 2, \text{ or } 3$ , M is an early transition metal, A is an A-group element and X is either carbon and/or nitrogen. According to crystal structures, they are further classified into 211, 312, and 413 phases with 211 being the most common. [25, 26]. Figure 1.1 shows the M, A, and X groups on the periodic table. Figure 1.2 shows schematic of the crystal structures of 211, 312, and 413 MAX phases. Table 1.1 lists different 211, 312, and 413 MAX phases known to date in both bulk and thin film form.

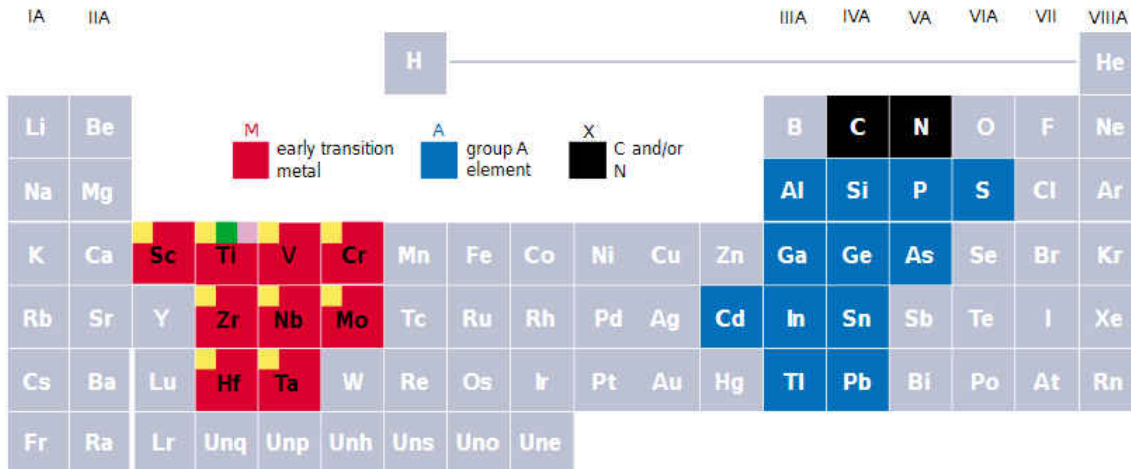


Figure 1.1 The MAX phases consist of an early transition metal M (red) in the periodic table, an element from the A group, usually IIIA and IVA (dark blue), and a third element, X, which is either nitrogen or carbon (black), in the composition  $M_{n+1}AX_n$ , where n is 1, 2 or 3. [27]

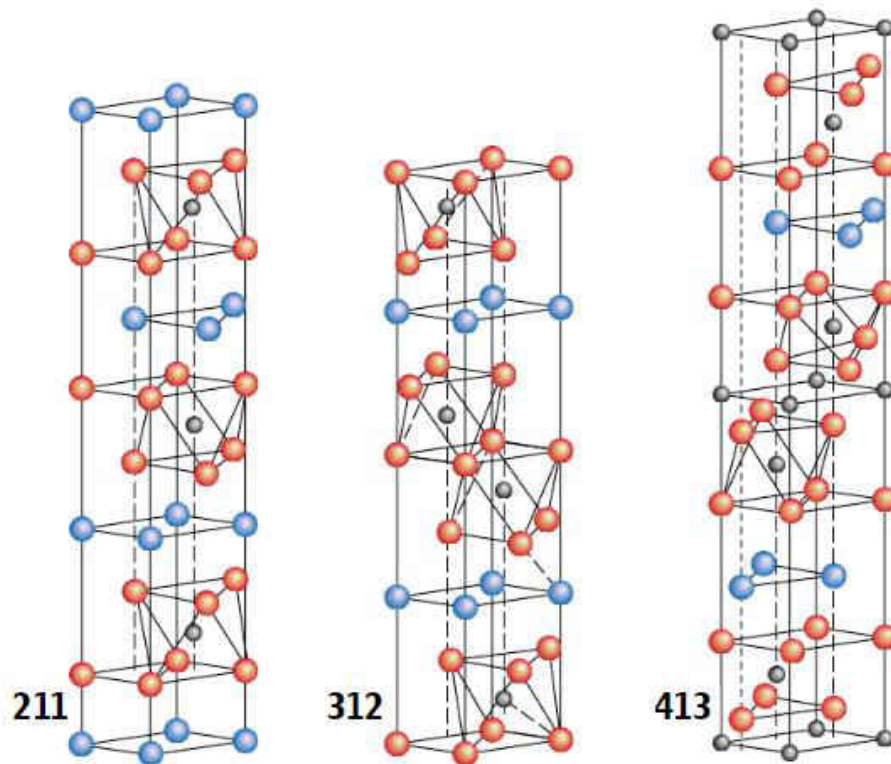


Figure 1.2 Crystal Structure of the 211, 312, and 413 MAX phases [27]

Table 1.1 A list of MAX phases known to date, in both bulk and thin film form [28, 29]

211	$\text{Sc}_2\text{AlC}$ , $\text{Sc}_2\text{GaC}$ , $\text{Sc}_2\text{InC}$ , $\text{Sc}_2\text{AlTiC}$ , $\text{Ti}_2\text{AlC}$ , $\text{Ti}_2\text{AlN}$ , $\text{Ti}_2\text{SiC}$ , $\text{Ti}_2\text{PC}$ , $\text{Ti}_2\text{SC}$ , $\text{Ti}_2\text{GaC}$ , $\text{Ti}_2\text{GaN}$ , $\text{Ti}_2\text{GeC}$ , $\text{Ti}_2\text{AsC}$ , $\text{Ti}_2\text{CdC}$ , $\text{Ti}_2\text{InC}$ , $\text{Ti}_2\text{InN}$ , $\text{Ti}_2\text{SnC}$ , $\text{Ti}_2\text{TlC}$ , $\text{Ti}_2\text{PbC}$ , $\text{V}_2\text{AlC}$ , $\text{V}_2\text{SiC}$ , $\text{V}_2\text{PC}$ , $\text{V}_2\text{GaC}$ , $\text{V}_2\text{GaN}$ , $\text{V}_2\text{GeC}$ , $\text{V}_2\text{AsC}$ , $\text{Cr}_2\text{AlC}$ , $\text{Cr}_2\text{GaC}$ , $\text{Cr}_2\text{GaN}$ , $\text{Cr}_2\text{GeC}$ , $\text{Zr}_2\text{AlC}$ , $\text{Zr}_2\text{AlN}$ , $\text{Zr}_2\text{SC}$ , $\text{Zr}_2\text{InC}$ , $\text{Zr}_2\text{InN}$ , $\text{Zr}_2\text{SnC}$ , $\text{Zr}_2\text{TlC}$ , $\text{Zr}_2\text{TlN}$ , $\text{Zr}_2\text{PbC}$ , $\text{Nb}_2\text{AlC}$ , $\text{Nb}_2\text{PC}$ , $\text{Nb}_2\text{SC}$ , $\text{Nb}_2\text{GaC}$ , $\text{Nb}_2\text{InC}$ , $\text{Nb}_2\text{SnC}$ , $\text{Nb}_2\text{AsC}$ , $\text{Mo}_2\text{GaC}$ , $\text{Hf}_2\text{AlC}$ , $\text{Hf}_2\text{AlN}$ , $\text{Hf}_2\text{SC}$ , $\text{Hf}_2\text{InC}$ , $\text{Hf}_2\text{SnC}$ , $\text{Hf}_2\text{SnN}$ , $\text{Hf}_2\text{TlC}$ , $\text{Hf}_2\text{PbC}$ , $\text{Ta}_2\text{AlC}$ , $\text{Ta}_2\text{GaC}$ ,
312	$\text{Ti}_3\text{AlC}_2$ , $\text{Ti}_3\text{GaC}_2$ , $\text{Ti}_3\text{InC}_2$ , $\text{V}_3\text{AlC}_2$ , $\text{Ti}_3\text{SiC}_2$ , $\text{Ti}_3\text{GeC}_2$ , $\text{Ti}_3\text{SnC}_2$ , $\text{Ta}_3\text{AlC}_2$ , $\text{Zr}_3\text{AlC}_2$ , $\text{V}_3\text{SiC}_2$ , $\text{Nb}_3\text{SiC}_2$
413	$\text{Ti}_4\text{AlN}_3$ , $\text{V}_4\text{AlC}_3$ , $\text{Ti}_4\text{GaC}_3$ , $\text{Ti}_4\text{SiC}_3$ , $\text{Ti}_4\text{GeC}_3$ , $\text{Nb}_4\text{AlC}_3$ , $\text{Ta}_4\text{AlC}_3$

These solids are bestowed with exciting properties, for example, they are elastically stiff, exceptional thermally and electrical conductors, oxidation resistant, resistant to chemical attack, and have relatively low thermal expansion coefficients. In addition, they are machinable and are highly damage tolerant [25, 26].

Due to their unique combination of properties, MAX phases can have a wide variety of applications. Some of the potential applications are:

- Replacement of graphite for high temperature applications, for example MAX phases such as  $\text{Ti}_2\text{AlC}$  have several advantages over graphite such as better wear and oxidation resistance. In addition, it also has high strengths, moduli and thermal conductivities which can be considered further positive attributes.
- Heating elements as MAX phases form stable and protective oxide. These heating elements in air, argon, hydrogen, or vacuum.

- High temperature foil bearings and other tribological applications because of the self-lubricating nature of the material.
- Gas burner nozzles as they form protective passivating layer. In addition, as compared to traditional ceramics they can be easily joined. Furthermore, they can be readily threaded and can potentially replace metallic nozzles.
- Tools for dry drilling of concrete where diamonds can be embedded in a  $Ti_3SiC_2$  matrix.
- $Ti_3SiC_2$  can be used as glove and condom formers.
- Nonstick coating for cookware as they are durable, stick and stain resistant, thermal shock resistant, and dishwasher safe for use in cookware, cutlery, and other cooking utensils.
- $Ti_3AlC_2$  and  $Ti_3SiC_2$  are quite resistant to radiation damage. They can be coated on Zircaloy tubes so that they can form a thin cohesive and adhesive alumina layer to protect the tubes in case of accident due to loss of coolant. Also,  $Ti_3SiC_2$  doesn't react with molten Pb or Pb-Bi alloys so it could be a good material for ladle containing molten Pb or Pb-Bi alloys in nuclear reactors.
- Conductive element in spark plugs and other ignition devices.
- Sputtering targets for the deposition of electrical contacts.
- Electrical contact for SiC-based devices where they can be used harsh environments.
- Substrates for ruthenium oxide and sulfide-based catalysts for different electrochemical applications [25, 26].

### 1.3 MAB Phases

“MAB” phases are Boron containing ternary [30, 31]. Kota et al. [31] synthesized and characterized bulk polycrystalline MoAlB ceramics by using a single step reactive hot-pressing technique. They observed that MoAlB forms dense and adherent alumina scales during static

oxidation up to at least 1300°C. They also showed that these solids have high thermal conductivity and its thermal expansion coefficient ( $9.5 \times 10^{-6} \text{ K}^{-1}$ ) makes it compatible with many engineering alloys. It had high compressive strength and relatively low hardness. All of these properties show that MoAlB ceramics can have applications in high temperature materials and coatings [31].

Recently, Benamor et al. [32] investigated the dry sliding friction and wear behavior of fully dense, single-phase MoAlB against alumina and 100Cr6 steel counterparts. Their group observed that friction coefficient was load sensitive during testing against alumina. Detailed SEM studies showed that the abrasion was the dominant wear mechanism. Against steel, they found that the friction coefficient decreased with increasing load and the wear rates were low under all applied loads. This study clearly shows the excellent wear properties of the MoAlB.

#### 1.4 Additive Manufacturing

Additive manufacturing (AM) is a manufacturing process that uses computer-aided-design (CAD) software or 3D object scanners to communicate with a machine that deposits material, layer upon layer, into highly precise geometric shapes. The name additive manufacture comes from the fact that the process is accomplished by adding the material layer by layer to create the desired object. In contrast to traditional methods, where excess material has to be removed through milling, machining, carving, shaping etc. [33]

Several different types of materials can be used in the AM process including metal powders, thermoplastics, ceramics, composites, glass, and even edibles such as chocolate. The AM process first starts with the creation of an object that is digitally defined in a CAD program. The object is saved as a stereolithography file or .stl file that essentially “slice” the object into ultra-thin layers. The information from this file guides the nozzle or print head with precise motions along a specific path to deposit material layer-by-layer until a completed part is achieved, or with

selective laser melting/sintering a laser or electron beam selectively melts or partially melts in a bed of powdered material. As the materials cool or cure, depending on the type of AM, they fuse together to form a 3-dimensional structure. [33]

The term additive manufacturing encompasses a variety of different processes and is typically used interchangeably with the term 3D printing. These processes include material extrusion, directed energy deposition, material jetting, binder jetting, sheet lamination, vat photopolymerization and powder bed fusion. There are many different applications of AM. AM is well suited for the production of light-weight, complex geometric designs for applications in the aerospace industry. They also have applications in the automotive industry by printing aluminum alloys to produce exhaust pipes and pump parts and with various polymers to produce bumper parts. Some medical applications of 3D printing include printing of bone grafts and synthetic organs. [33]

Material extrusion is one of the most well-known AM techniques. This process functions by drawing material through a nozzle mounted on a moveable arm. The material is deposited on a moveable platform, where it is built up layer-by-layer, with the nozzle moving in a horizontal motion and the moveable platform moving vertically and, in some cases, horizontally. Layer adhesion occurs by temperature control and in some cases chemical bonding agents are used. [33]

Fused Deposition Modeling (FDM), a type of material extrusion, builds 3D objects by selective deposition of melted material in a pre-determined path layer-by-layer. Typically, thermoplastic polymer filaments are the material used for this manufacturing technique. Some advantages of this type of AM are that it is a cost-effective method to produce custom parts and prototypes, there is a high availability of the technology so lead times are short, and a wide range of thermoplastic filaments are available. There are also disadvantages of using this type of AM.

Some disadvantages include the lowest dimensional accuracy and resolution when compared to other 3D printing technologies, parts made by FDM are likely to have visible layer lines, so post processing is needed to obtain a smooth finish, and their layer adhesion makes the FDM parts anisotropic, so this method of AM is not recommended for mechanically critical components. [34, 35]

Material Jetting, another a type of AM, is a process in which material is jetted onto a build platform using either a continuous or Drop on Demand (DOD) approach. DOD is a method of material jetting in which each layer is allowed to dry before depositing an additional layer. Layers are either allowed to cool and harden or are cured by UV light. Some post processing is usually required to remove support material. Typically, photopolymer resin is used with this manufacturing technique. An important advantage of material jetting is its ability to produce highly accurate multi-material and multi-color prints and, in some cases, can be post processed to 100% transparency. It can also simulate injection-molded parts. The printing process is also sterilizable which is highly advantageous for medical applications. [36]. The rest of the thesis is organized into three chapters: (a) Chapter II is focused with designing PLA-Lignin composites by using “drop on demand” 3D printing process, (b) Chapter III is focused on designing novel MAX/MAB-PLA composites by FDM, and (c) Chapter IV focuses on future work and recommendations as a result of this thesis.



## **CHAPTER II**

### **LIGNIN/PLA AM COMPOSITES**

This work was included in the patent application titled “Method of Fabricating Lignin Based Polymeric Systems”. File date: February 16, 2018, Application No. 15/932,226. K&L File No. U66-012062, UND File No.: UND 16-09. US Patent Application of Surojit Gupta et al.

#### 2.1 Introduction

Cost-effective, reliable methods for the conversion and application of lignin are technically challenging due to lignin’s recalcitrant nature but used in small amounts it can be utilized as a filler in various polymer matrices. This presents an opportunity to utilize a readily available material as a cost effective and environmentally friendly filler in a polymer matrix such as Polylactic acid (PLA), a biodegradable polymer made from corn.

In particular, lignin can be used to create a “green” or environmentally friendly polymer composite using a non-polar polymer matrix and as-received lignin particulates with no chemical treatments or additives to create polymer-lignin composite layers formed using three-dimensional printing technology. For instance, a prepared PLA-lignin composite solution can be loaded into a three-dimensional printer and additively manufactured into the desired shape or layer.

## 2.2 Experimental

In order to manufacture the lignin/PLA composites, a liquid mixture of the two was made. This mixing process was accomplished by using a volatile solvent to dissolve the PLA to allow the lignin to become well mixed in the PLA matrix. The process of making this mixture included using 50 wt% untreated lignin powder to 50 wt% PLA pellets (a product from Filabot, PLA supplier is NatureWorks) for a total of 10 grams (5 g of lignin and 5 g of PLA). The two were combined in a mixing container with 50 mL of dichloromethane (DCM). A magnetic stir bar was placed in the mixing container and the container was sealed with a lid. The mixing container was placed on a magnetic stir plate and stirred at room temperature for 2 hours at a set speed. After the mixing was completed, the mixture was then loaded into the printer and the printing process was started.

The printer that was used in this experiment was a Hyrel engine SR- standard resolution 3D printer. The printer head was a VOL-25 extruder, capable of heating up to 100 °C, with an anodized aluminum syringe with a 25-cc capacity. The nozzle diameter on the syringe was 1.5-mm. Print speed was 600 mm/min and layer thickness was 0.5 mm. Some of the tech specs include:

- Build volume: x-axis 225 mm, y-axis 200 mm, z-axis 200 mm
- Positional accuracy: x-axis  $\pm 50 \mu\text{m}$ , y-axis  $\pm 150 \mu\text{m}$ , z-axis  $\pm 10 \mu\text{m}$
- Positional resolution: x-axis  $5 \mu\text{m}$ , y-axis  $5 \mu\text{m}$ , z-axis  $1 \mu\text{m}$
- Chassis: Powder-coated Steel & Anodized Aluminum (no enclosure)
- Motion control:
  - Precision Ball Screw in X, Y, and Z Axes
  - Precision Linear Bearing System in X, Y, and Z Axes

- Electronics:
  - State-of-the-art 150+ MHz 32-bit ARM processor
  - Modular, micro-stepping motor-drivers with closed-loop encoding
  - Integrated, Dual CAN-bus architecture
  - “Smooth Move” motion control technology firmware
  - Integrated camera [37]

A preprogrammed STL file was used for the prints. It was a rectangular prism, with the x and y directions being equal and the z direction being much smaller. The print dimensions that were made include: (X, Y, and Z directions respectively)

- 50 mm x 50 mm x 2 mm
- 50 mm x 50 mm x 4 mm
- 50 mm x 50 mm x 6 mm
- 75 mm x 75 mm x 2 mm
- 100 mm x 100 mm x 2 mm

Figure 2.1 depicts, (a) the printer in the middle of a print and (b) a completed 3D printed sample. The printed samples were cured on the print stage overnight and were then oven dried at 100°C for 24 hours to remove any remaining DCM. Tensile test coupons were cut from the dried samples for testing. Tensile tests were performed with a Shimadzu Universal Testing Machine (Shimadzu AG-IS UTM, Shimadzu Scientific Instruments Inc., Columbia, MD). A 5 kN load cell was used for testing with a test speed of 5 mm/min.

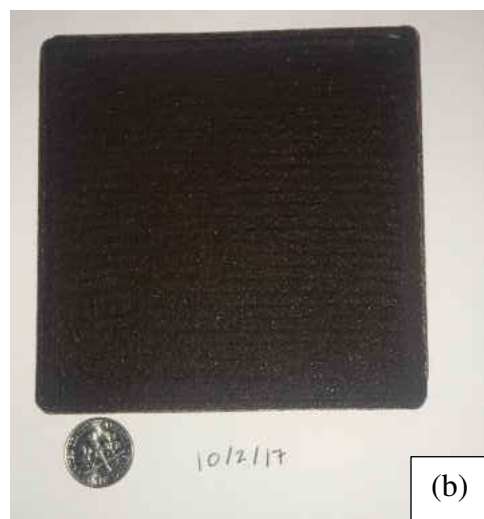


Figure 2.1: Schematics of, (a) a 3D printer printing PLA-50 wt% Lignin composition, and (b) a PLA-50 wt% Lignin 3D printed sample.

Throughout the printing experiment, several issues were encountered. One of the issues included the samples sticking to the glass sample stage. This issue was never fully resolved, but several attempts were made to alleviate this problem. Some attempts at resolving it included cleaning the glass with acetone prior to printing (with no success), using water to remove the sample after it had dried overnight (one of the more effective attempts, worked better with thicker samples), and using a releasing agent on the glass prior to printing (unsuccessful in aiding the sample removal). If further experiments of this type are done in the future, another method of removal to attempt would be putting the glass that the samples were stuck to in the drying oven to test if it was the residual DCM that was causing the samples to adhere to the glass sample stage.

Another problem that was encountered was syringe under- or over-extrusion. For a few of the print attempts, over-extrusion of the print material occurred causing the print to fail as the amount of material extruded was not held constant. Also, with other attempts, problems with under-extrusion occurred, where the print material was not coming out in enough volume to make a new layer. Initially, these were thought to be an issue with the viscosity of the print material, so the ratio of solvent to solute was changed to increase or decrease the viscosity. There was no success with changing the viscosity of the print material. It was later discovered that after several uses, the O-ring that seals the syringe had been partially torn from repeated use. Once the O-ring was replaced, the issues with under- or over-extrusion were resolved.

### 2.3 Results and Discussion

The 3D printed samples were compared with solvent-cast samples. The tensile data from the 3D printed and solvent-cast samples is compared in Figure 2.2. From the tensile stress vs displacement plot, it can be seen that the 3D printed samples behave similarly to the solvent-cast samples. All 3D printed PLA-lignin composite samples exhibited similar behavior, which is summarized in Table 2.1.

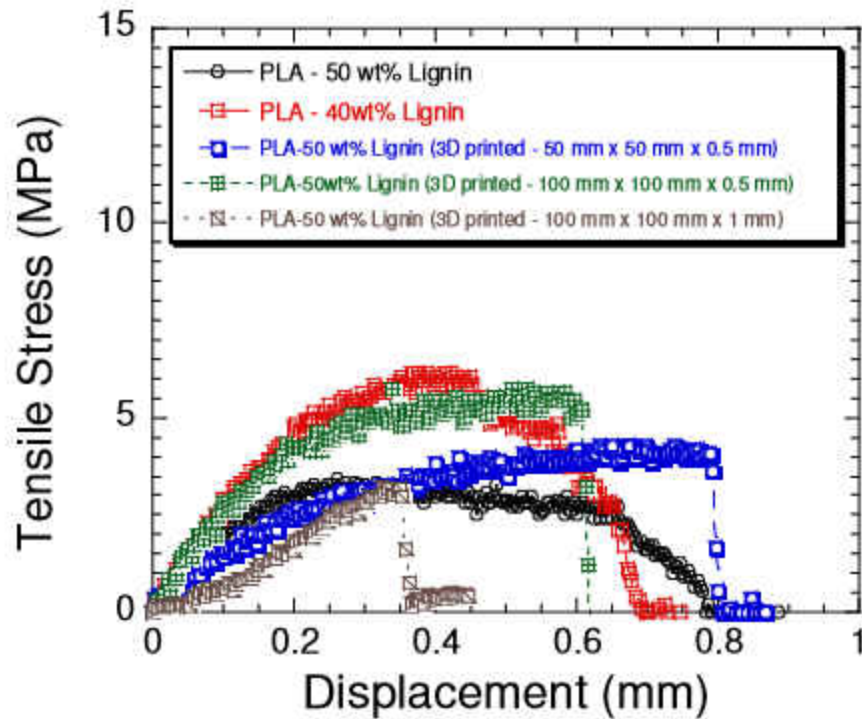


Figure 2.2 Tensile Stress vs Displacement of 3D Printed and Solvent-Cast PLA-Lignin Composites.

Table 2.1 Summary of the Tensile Strengths of 3D printed PLA-lignin composites

Sample	3D Printing Size	Average Tensile Strength
PLA 50 wt% lignin	50 mm x 50 mm x 0.5 mm	4.34 MPa
PLA 50 wt% lignin	100 mm x 100 mm x 1 mm	3.40 MPa
PLA 50 wt% lignin	100 mm x 100 mm x 0.5 mm	5.07 MPa

## 2.4 Conclusions

A novel method of manufacturing 3D printed samples by using liquid inks based of PLA was developed. The mechanical behavior of the PLA-Lignin composites were studied. It was observed that the 3D printed samples performed similarly to as-cast samples of the same composition. Also, some of the 3D printed samples had a much longer plastic region than the as-

cast samples. Further studies are needed to determine if the print dimension plays a significant role on the plastic behavior of the 3D printed samples.

## **CHAPTER III**

### **SYNTHESIS AND CHARACTERIZATION OF NOVEL MAX/MAB POLYMER COMPOSITES BY FUSED DEPOSITION MODELLING (FDM)**

#### **3.1 Introduction**

This chapter describes the synthesis and characterization of MAX-PLA composites and MAB-PLA composites. As a nomenclature, MAXPOLs are composite materials composed of MAX phases dispersed in a polymer matrix base. Similarly, MABPOLs are composed of MAB phases dispersed in polymer matrix. If the volume concentration of MAX or MAB phases are less than 30 vol% then they will be described as MAX reinforced polymers (MRPs) or MAB reinforced polymers (MBRPs). Please note, MRPs or MBRPs are a sub-category of MAXPOLs or MABPOLs, respectively. In the rest of thesis, the composites designed during study will be referred to as MRPs or MBRPs.

#### **3.2 Experimental**

Filaments composed of various MAX and MAB phases incorporated into the PLA matrix were synthesized. Nine compositions of filament were made in this study. The compositions and nomenclature used are shown in Table 3.1.



Table 3.1 Materials extruded along with their composition and nomenclature used.

Material Extruded	Composition	Nomenclature
Pure PLA	100 wt% PLA	PLA
MoAlB/PLA	1 wt% (0.19 vol%) MoAlB-99 wt% (99.81 vol%) PLA	PLA-1 wt% MoAlB
	5 wt% (0.97 vol%) MoAlB-95 wt% (99.03 vol%) PLA	PLA-5 wt% MoAlB
$Ti_3AlC_2$ /PLA	1 wt% (0.3 vol%) $Ti_3AlC_2$ -99 wt% (99.70 vol%) PLA	PLA-1 wt% $Ti_3AlC_2$
	5 wt% (1.5 vol%) $Ti_3AlC_2$ -95 wt% (98.50 vol%) PLA	PLA-5 wt% $Ti_3AlC_2$
$Ti_3SiC_2$ /PLA	1 wt% (0.28 vol%) $Ti_3SiC_2$ -99 wt% (99.72 vol%) PLA	PLA-1 wt% $Ti_3SiC_2$
	5 wt% (1.43 vol%) $Ti_3SiC_2$ -95 wt% (98.57 vol%) PLA	PLA-5 wt% $Ti_3SiC_2$
$Cr_2AlC$ /PLA	1 wt% (0.24 vol%) $Cr_2AlC$ -99 wt% (99.76 vol%) PLA	PLA-1 wt% $Cr_2AlC$
	5 wt% (1.24 vol%) $Cr_2AlC$ -95 wt% (98.76 vol%) PLA	PLA-5 wt% $Cr_2AlC$

The PLA used in this study was pulverized PLA-4043D obtained from Filabot located in Barre, VT.  $Ti_3SiC_2$  powder (-325 mesh) was obtained from Kanthal, Hallstahammar, Sweden. The MoAlB powders (-325 mesh) [38],  $Cr_2AlC$  powder (-325 mesh) [39] and  $Ti_3AlC_2$  powders (-325 mesh) [40] were fabricated in-house. Each batch of filament was made by first preparing 100 g batches of each composition. Due to size limitations of the ball mill mixing containers, the 100 g batches were made in four 25 g portions. The 25 g mixtures are as follows: the 1 wt% mixture consisted of 0.25 g of MAX or MAB powder and 24.75 g of the pulverized PLA powder and the 5 wt% mixtures consisted of 1.25 g of MAX or MAB powder and 23.75 g of the pulverized PLA powder. Polymethyl methacrylate (PMMA) mixing containers and three PMMA mixing balls per container were used to mix the 25 g powder mixtures. The powders were mixed by dry ball milling (8000 M mixer Mill, SPEX SamplePrep, Metuchen, NJ) for 5 minutes. The 100 g mixtures were stored in plastic containers until they were ready to be extruded.

An extruder (Filabot EX2 extruder, Filabot, Barre, VT) was used for making the filament in this set of tests. The extruder was set to 175 °C to extrude pure PLA powder. Approximately 100 g of useable PLA filament was made before using the MAXPOL or MABPOL mixtures to ensure there was enough useable PLA filament for any test coupons to be printed. Before a new composition was run through the extruder, any remaining powder from the previous composition was vacuumed out of the hopper and any powder that the vacuum could not get was wiped out with a slightly damp paper towel. Then the hopper was filled  $\frac{1}{4}$  or  $\frac{3}{4}$  full, depending on what the previous composition was, with PLA pellets to flush out the previous composition in the extruder. The hopper was filled  $\frac{1}{4}$  full for cleaning between compositions of the same powder type to distinguish the transition to the new filament composition and  $\frac{3}{4}$  full between compositions of different powder type to ensure the previous powder was flushed out of the system. PLA pellets were used for this cleaning process to save the pulverized PLA powder for the powder mixtures. The powder and pellets were of the same type (product number 4043D, Filabot, Barre, VT).

When extruding, the filament comes out very hot and the force of gravity combined with the weight of the filament can stretch the filament thinner than the required  $1.75\text{mm}\pm 0.05\text{mm}$  filament diameter range. To control this, the drop height of the filament and cooling fan placement height were crucial to optimize. The drop height is the height of the extruder at table height, 98.5 cm ( $38\frac{3}{4}$  in), minus the stand height. The fan height is the height taken from the bottom of the fan to the floor or is stated as the fan sitting directly on top of the stand making the stand height and fan height the same. The drop height and fan height were different between the compositions extruded, and it should be noted that the additives lowered the extrusion temperature of PLA.

Initially, boxes were used to obtain optimal drop heights, but an adjustable stand was made so that an easily adjustable platform was available for the filament to land on. An easily adjustable stand allowed for the drop height to be optimized for each type of filament being extruded. The adjustable stand was made from ½ inch PVC pipe, 4-½ inch corner connectors for the PVC pipe, 5 clamps (4 for holding the platform and 1 for holding the fan), 1 flat 12”x12” piece of wood to act as the surface for the filament to land on. The square piece of wood was covered with mylar tape to prevent the filament from singeing or sticking to the surface of the wood. Figure 3.1 is a schematic of the extruder set up (image of extruder from Filabot) [41].

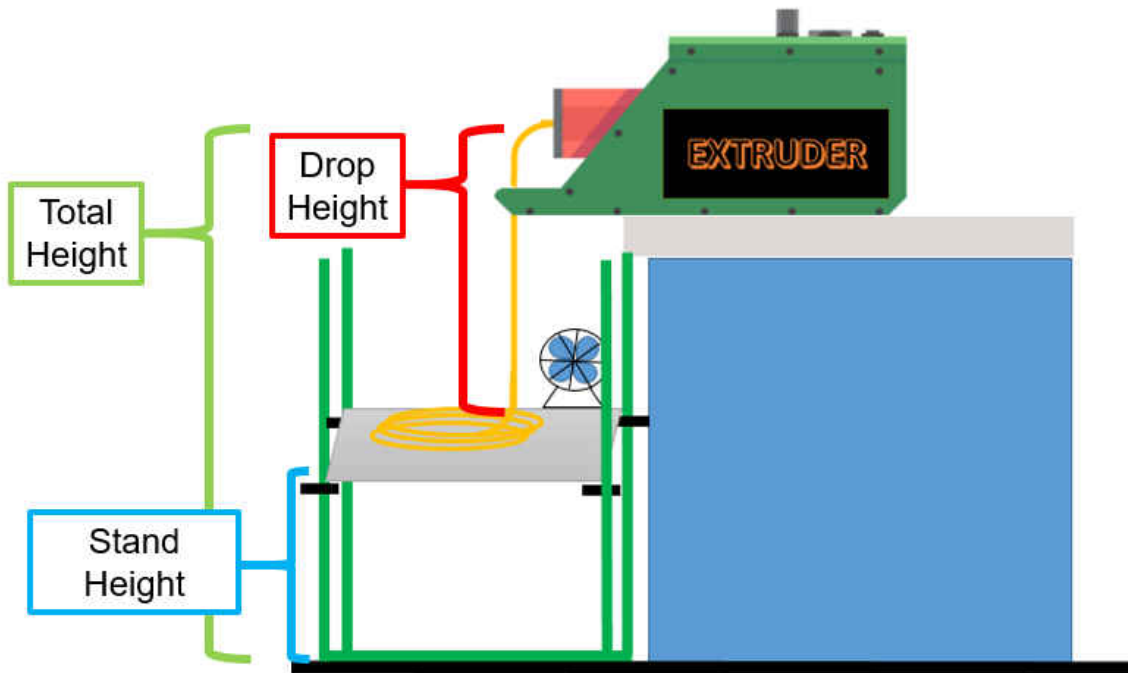


Figure 3.1: Schematics of the extruder used for designing filaments for 3D printing.

The temperatures were optimized for each filament based on the appearance of the filament at the varying temperature settings. The first composition to be tested for temperature optimization was 1 wt% MoAlB. During this process, the mixture was first extruded at 175°C, but the temperature was decreased in 5°C increments until the temperature was optimized at 165°C. The

higher temperatures were not suitable for this mixture because the consistency of the filament was fluidic, and the filament exhibited bubbling which is an indication that the temperature is set too high. This same process was repeated for each of the filaments until each of their individual settings were determined.

The stand height settings were done by guessing a height setting and checking if the filament was within the right range. This was done by choosing a height and allowing the filament to coil into 3 to 4 coils, turning off the extrude switch and measuring the filament diameter. When the stand height was set higher, the filament diameter increased, since it was closer to the extruder. When the stand height was set lower, the filament diameter decreased, since it was farther from the extruder. Stand height settings were measured during experimentation and drop height was calculated from the total height of the extruder (height from the extruder nozzle to the floor) minus the stand height.

It should be noted that the pure PLA filament that was extruded was done before drop height measurements were taken, but 100 g of useable filament was obtained. The temperature for pure PLA extrusion was optimal at 175°C. Filament optimization for the various filaments is shown in Table 3.2.

Table 3.2 Optimized settings for various filament compositions.

<b>Composition</b>	<b>Fan Height (cm)</b>	<b>Stand Height (cm)</b>	<b>Drop Height* (cm)</b>	<b>Temperature (°C)</b>
PLA	N/A	N/A	N/A	175
PLA-1wt% Ti <sub>3</sub> SiC <sub>2</sub>	49.5	49.5	49	175
PLA-5wt% Ti <sub>3</sub> SiC <sub>2</sub>	63.5	63.5	35	165
PLA-1wt% MoAlB	63.5	63.5	35	165
PLA-5 wt% MoAlB	63.5	63.5	35	165
PLA-1wt%Ti <sub>3</sub> AlC <sub>2</sub>	63.5	63.5	35	165
PLA-5wt% Ti <sub>3</sub> AlC <sub>2</sub>	63.5	63.5	35	165
PLA-1wt%Cr <sub>2</sub> AlC	63.5	63.5	35	165
PLA-5wt%Cr <sub>2</sub> AlC	63.5	63.5	35	165

\*Total height was 98.5 cm, total height – stand height = drop height

The 3D printer used to manufacture the test coupons was a FDM type printer (H400 3D printer, Afinia, Chanhassen, MN). Figure 3.2 is a picture of the printer used during this study. The filament size that is compatible with this printer must be  $1.75 \pm 0.05$  mm in diameter. Since this is such a tight range, it was important to measure the filament diameter properly to prevent damaging the printer head. To ensure that the prints were successful, every inch of filament was measured with multiple measurements done at the same points to ensure that the diameter was within the range.



Figure 3.2: Afinia H400 3-D printer [42]

All prints used the following settings: infill of 99%, layer thickness of 0.2 mm, quality set to normal, unsolid model, no raft and no support. STL files made by a previous student were used to print the test coupons. [43] The two coupon types were tensile coupons for tensile tests and cylindrical coupons for various surface tests. The dimensions of printing are shown in Figure 3.3.

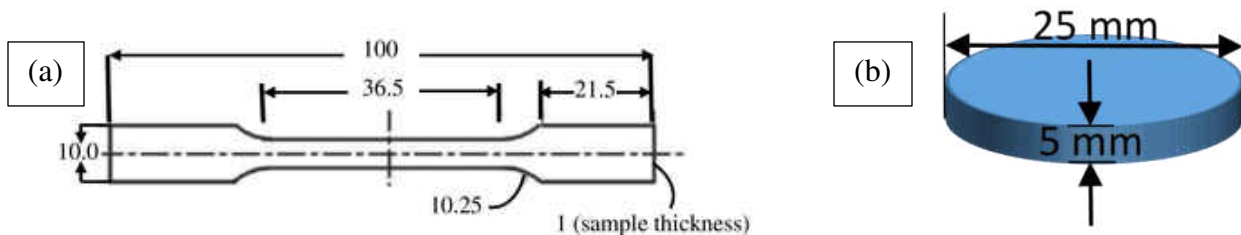


Figure 3.3 Sample dimensions for 3D printed testing coupons (a) tensile test coupon (dimensions in mm) (b) cylindrical test coupon [43]

To prepare the printer for printing the samples, mylar tape was placed on the printing platform to help sample adhesion, to prevent sample warping during printing and to help with removal after the print is complete. The printer platform was preheated for 30 mins before printing

or until it was preheated to 60°C. The filament was loaded into the printer head while the platform preheated (when printing duplicates the filament was kept in the head). The STL files were loaded on the print program while waiting for the printer to preheat so that printing could begin as soon as the print platform was heated sufficiently. The print was started once the print bed reached a sufficient temperature. The tensile coupons used approximately 1g of filament and the cylindrical coupons used approximately 3.5g of filament. After the print was completed, excess filament attached to the sample was removed. Three cylindrical samples were printed per composition and five tensile coupons were printed per composition.

The dimensions of the cylindrical samples were taken using a Vernier caliper. Three measurements of height and diameter at three different points were done. Mass measurements were taken with an analytical balance. Density ( $\rho_E$ ) and porosity were calculated from the mass and volume measurements. Theoretical calculations of density ( $\rho_{Th}$ ) of composites was calculated by using rule of mixture calculations from theoretical density of the individual components. The porosity of the samples are determined from the following equation.

$$P(\%) = \left(1 - \frac{\rho_E}{\rho_{Th}}\right) \text{----- (III a)}$$

Tensile tests were done with a Shimadzu Universal Testing Machine (Shimadzu AG-IS UTM, Shimadzu Scientific Instruments Inc., Columbia, MD). A 5 kN load cell was used for testing with a test speed of 5 mm/min. Hardness of the cylindrical samples was measured with a Vicker's micro-hardness indenter (Mitutoyo HM-112, Mitutoyo Corporation, Aurora, IL). A load of 4.9 N was applied for 15 s. The cylindrical samples were also used for wettability and tribology testing. All the samples were characterized by JEOL JSM-6490LV Scanning Electron Microscope (JEOL USA, Inc., Peabody, Massachusetts.) in Secondary electron (SE) and Backscattered Electrons (BSE) mode. X-ray information was also determined by using a Thermo Nanotrace Energy

Dispersive X-ray detector with a NSS-300e acquisition engine. If a region is delineated to be chemically uniform in the micron level then it will be identified with two asterisks as \*microconstituent\*. It is critical to note and emphasize that this region is not necessarily single phase and measurement is for qualitative comparison. The accuracy of measuring C is quite low during chemistry analysis by X-ray detector in SEM, thus the presence of C in microconstituents will be designated as {C<sub>x</sub>}.

The contact angle analysis was performed on the polished samples until ~1 μm finishing. For each composition, a set of 3 tests were performed on randomly chosen spots by using an angle analyzer (FTÅ 125, First Ten Angstroms, Inc., Portsmouth, VA). During testing, a sessile drop of deionized (DI) water was deposited on each spot from a needle (CAD7932-12EA, Sigma-Aldrich, gauge 20), and a snapshot was taken after 10 s. For each drop the baseline and the curve fitting was done manually, thereafter, the contact angle was measured by using the software FTA32.

Thermal behavior was studied by Differential Scanning Calorimetry (DSC Q1000, TA Instruments, New Castle, DE 19720). During DSC, samples were heated at 20 °C/min from RT to 200 °C (first cycle) then cooled to RT, thereafter it was again heated at 20 °C/min to 200 °C (second cycle). In this chapter, the DSC results are reported for second cycle.

The tribological behavior of the samples were investigated by using a pin-on-disc tribometer (CSM Instruments SA, Peseux, Switzerland) by using 100Cr6 stainless steel balls against the 3D printed disc. The experimental conditions used during these studies were 5 N, ~50 cm/s linear speed, ~10 mm track radius, and a sliding distance of 2000 m, respectively. All the 3D printed discs were also polished to a ~1 μm finishing which were confirmed by using a surface profilometer (Surfcom 480A, Tokyo Seimitsu Co. Ltd., Japan). In this thesis, the  $\mu_{\text{mean}}$  of the results is reported which calculated by taking average of mean friction coefficients of three data



sets of similar compositions. The WR was calculated by measuring the mass of the stainless steels balls and 3D printed samples before and after the testing by using a weighing scale (Model XA82/220/2X, Radwag Balances and Scales, Poland). The specific wear rate (WR) was calculated from:

$$WR = (m_i - m_f) / (\rho \cdot N \cdot d) \text{ ----- (IIIb)}$$

where,  $m_i$  is the initial mass,  $m_f$  is the final mass,  $\rho$  is density of the composite,  $N$  is the applied load, and  $d$  is the total distance traversed by the sample during the tribology testing [3-7]. The total WR from both the counterparts is reported in the text. After tribological testing, the discs were then coated with Au/Pd by using a Balzers SCD 030 sputter coater (BAL-TEC RMC, Tucson AZ USA). The coated samples were then mounted on aluminum mounts for investigations by microscopy.

### 3.3 Results and Discussion

Figure 3.4 shows the microstructure of extruded filaments after 3D printing. In all cases, MAX or MoAlB particulates are well dispersed in the matrix. Figure 3.5 summarizes the microstructure of the 3D printed samples. In all the samples MAX or MoAlB particulates are well dispersed in the microstructure. Interestingly, on closer inspections pore and/or voids were observed in the 3D printed samples (for example, Figs. 3.5 b, d, and f). These results were further corroborated as all the 3D printed samples were porous, for example 3D printed PLA samples were ~90% dense as compared to PLA-1wt%Ti<sub>3</sub>SiC<sub>2</sub> and PLA-5wt%Ti<sub>3</sub>SiC<sub>2</sub> which were ~93% dense (Fig. 3.6). Comparatively, PLA-MoAlB and PLA-Ti<sub>3</sub>AlC<sub>2</sub> had similar porosity as PLA, whereas PLA-1wt%Ti<sub>3</sub>AlC<sub>2</sub> and PLA-5wt%Ti<sub>3</sub>AlC<sub>2</sub> had slightly higher porosity of ~13.5% and ~12.2%, respectively.

The hardness of PLA was ~160 MPa, and it marginally increased to ~167 MPa, ~171 MPa, and ~171 MPa in PLA-5wt%MoAlB, PLA-5wt%Ti<sub>3</sub>SiC<sub>2</sub>, and PLA-5wt%Ti<sub>3</sub>AlC<sub>2</sub>, respectively. However, PLA-5wt% Cr<sub>2</sub>AlC had similar value of ~161 MPa. Figure 3.7 summarizes the DSC profile of PLA and its composites during second heating cycle. PLA showed predominantly amorphous behavior with T<sub>g</sub> (glass transition temperature) at ~63 °C and melting point (MP) at ~150 °C. The addition of all the MAX phases promoted crystallization except PLA-1wt%Ti<sub>3</sub>SiC<sub>2</sub> which was predominantly amorphous. In addition, a sharp crystallization temperature (T<sub>c</sub>) peak was observed at ~105 °C except PLA-1wt%Ti<sub>3</sub>SiC<sub>2</sub>. Due to crystallization, the melting point of MRPs also increased to ~169 °C as compared to PLA. Comparatively, the addition of MoAlB did not change the characteristics of PLA, and MBRPs showed similar characteristics as PLA. Based on these results, it can be summarized that MAX Phases are promoting heterogenous crystallization of PLA matrix. In literature, Bindhu et al. [44] have also seen heterogenous crystallization in PLA matrix by adding ultrasonically exfoliated Boron Nitride (BN).

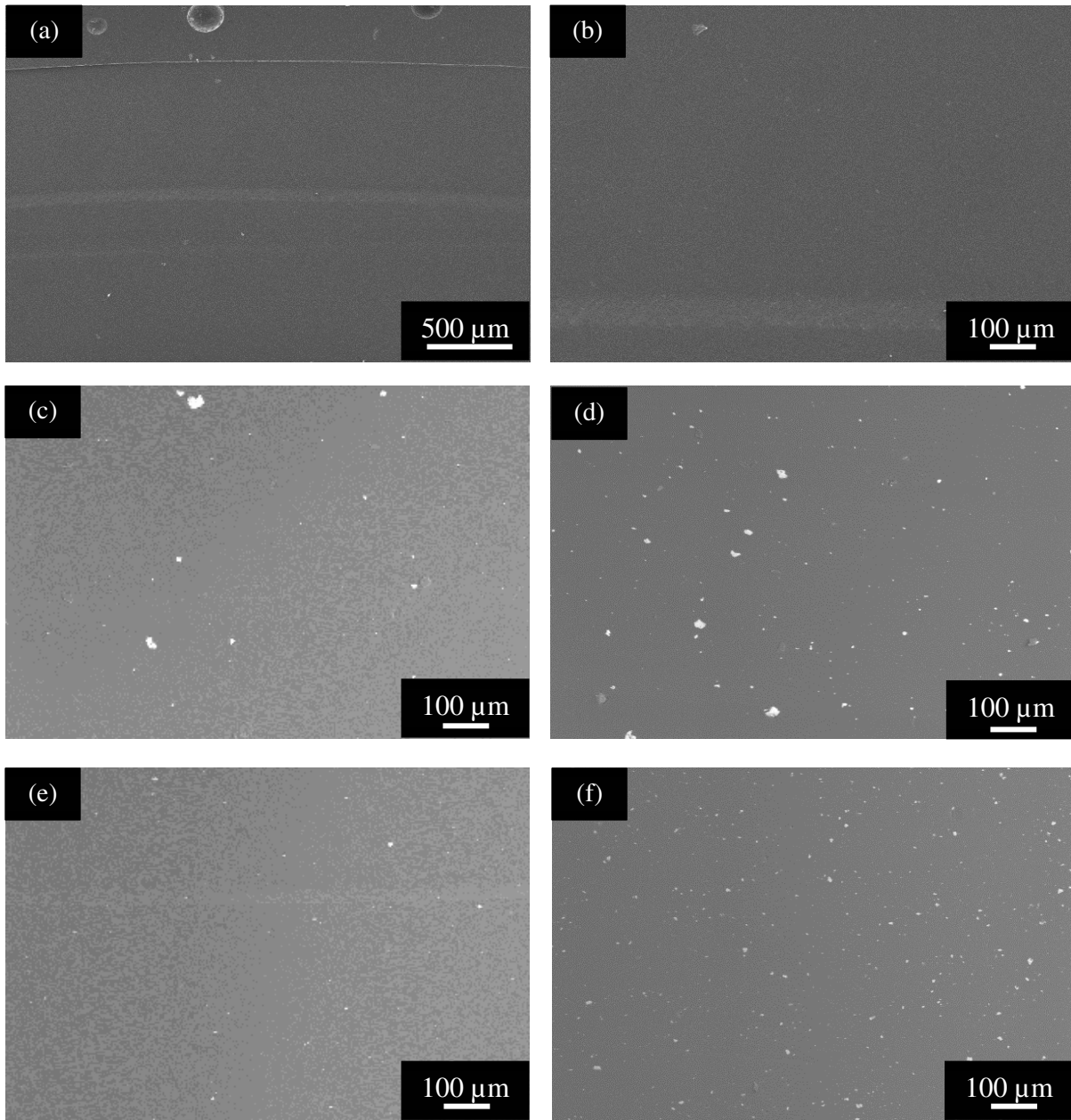


Figure 3.4: SEM micrographs of extruded filaments of, (a) PLA in SE, and BSE images of, (b) BSE of (a), (c) PLA-1wt% MoAlB, (d) PLA-5wt% MoAlB, (e) PLA-1wt% Ti<sub>3</sub>SiC<sub>2</sub>, (f) PLA-5wt% Ti<sub>3</sub>SiC<sub>2</sub>, (g) PLA-1wt% Ti<sub>3</sub>AlC<sub>2</sub>, (h) PLA-5wt%Ti<sub>3</sub>AlC<sub>2</sub>, (i) PLA-1wt%Cr<sub>2</sub>AlC, and (j) PLA-5wt%Cr<sub>2</sub>AlC

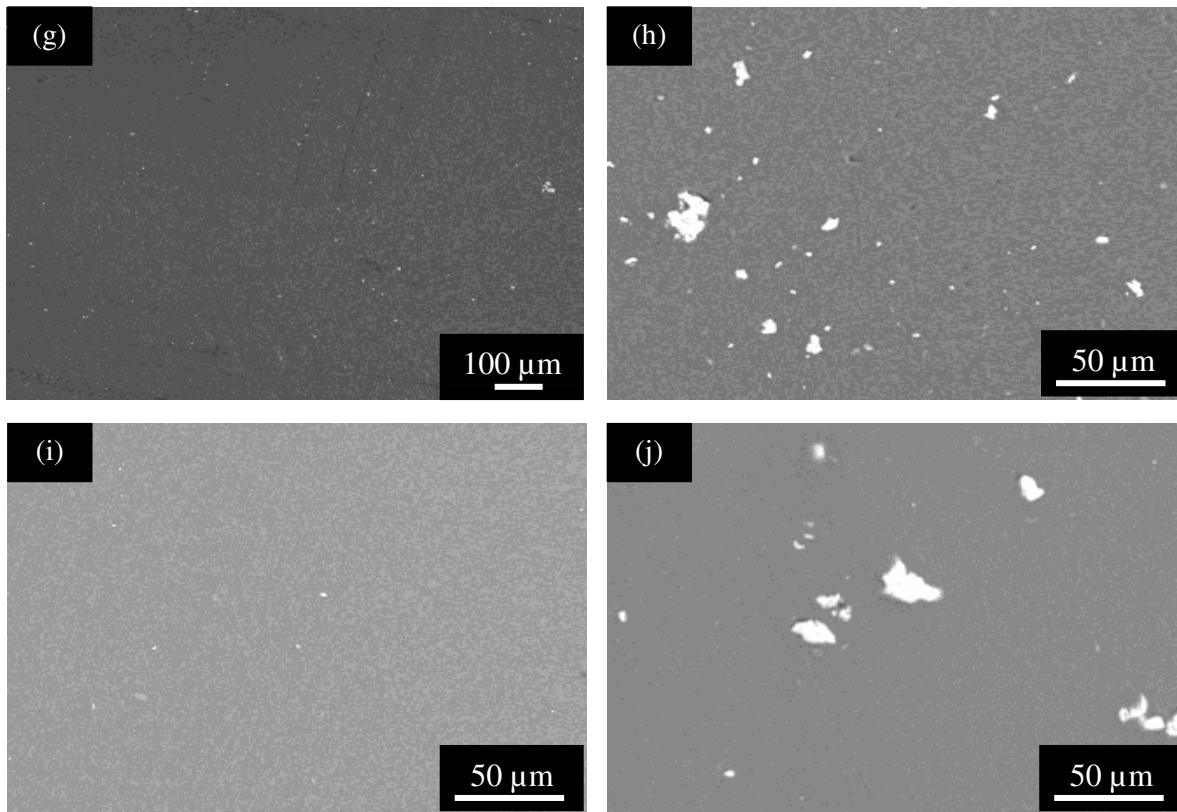


Figure 3.4: SEM micrographs of extruded filaments of, (a) PLA in SE, and BSE images of, (b) BSE of (a), (c) PLA-1wt% MoAlB, (d) PLA-5wt% MoAlB, (e) PLA-1wt%  $Ti_3SiC_2$ , (f) PLA-5wt%  $Ti_3SiC_2$ , (g) PLA-1wt%  $Ti_3AlC_2$ , (h) PLA-5wt%  $Ti_3AlC_2$ , (i) PLA-1wt%  $Cr_2AlC$ , and (j) PLA-5wt%  $Cr_2AlC$

Figure 3.8 shows a typical stress versus displacement plot of 3D printed PLA. The ultimate strength at which the material fractures is defined as Ultimate Tensile Strength (UTS). It is interesting to note that yielding was observed in the 3D samples. Rodríguez-Panes et al. [45] have observed similar yielding in 3D printed PLA samples. They also observed that thickness of layers, infill, and orientation had an impact on 3D printed PLA samples. In this Chapter, the infill and layer thickness were set at 99% and 0.2 mm, respectively. It is recommended that the effect of infill and layer thicknesses can be further studied in these composites.

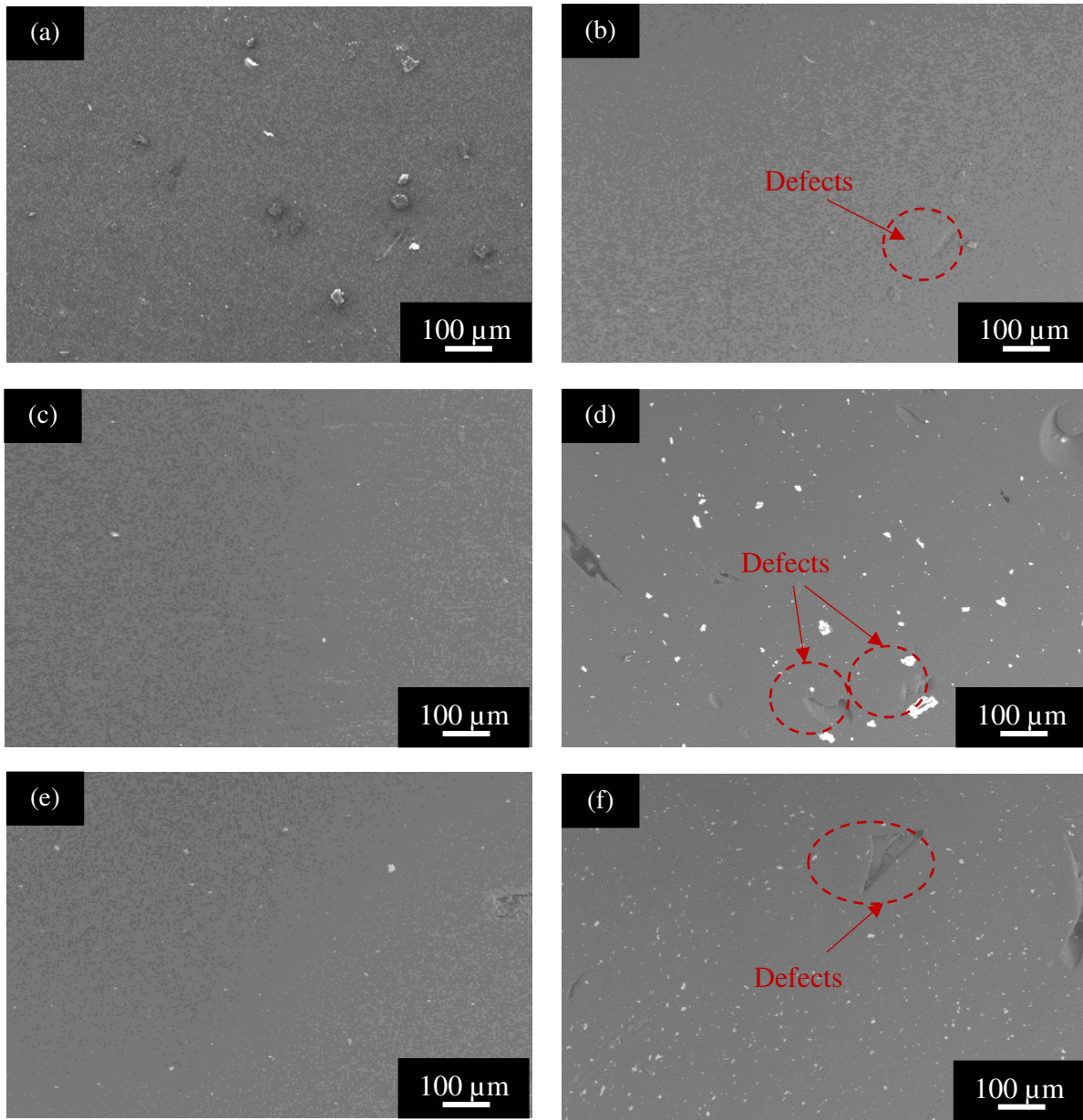


Figure 3.5: SEM micrographs of 3D printed, (a) PLA in SE, and BSE images of, (b) BSE of (a), (c) PLA-1wt% MoAlB, (d) PLA-5wt% MoAlB, (e) PLA-1wt% Ti<sub>3</sub>SiC<sub>2</sub>, (f) PLA-5wt% Ti<sub>3</sub>SiC<sub>2</sub>, (g) PLA-1wt% Ti<sub>3</sub>AlC<sub>2</sub>, (h) PLA-5wt%Ti<sub>3</sub>AlC<sub>2</sub>, (i) PLA-1wt%Cr<sub>2</sub>AlC, and (j) PLA-5wt%Cr<sub>2</sub>AlC.

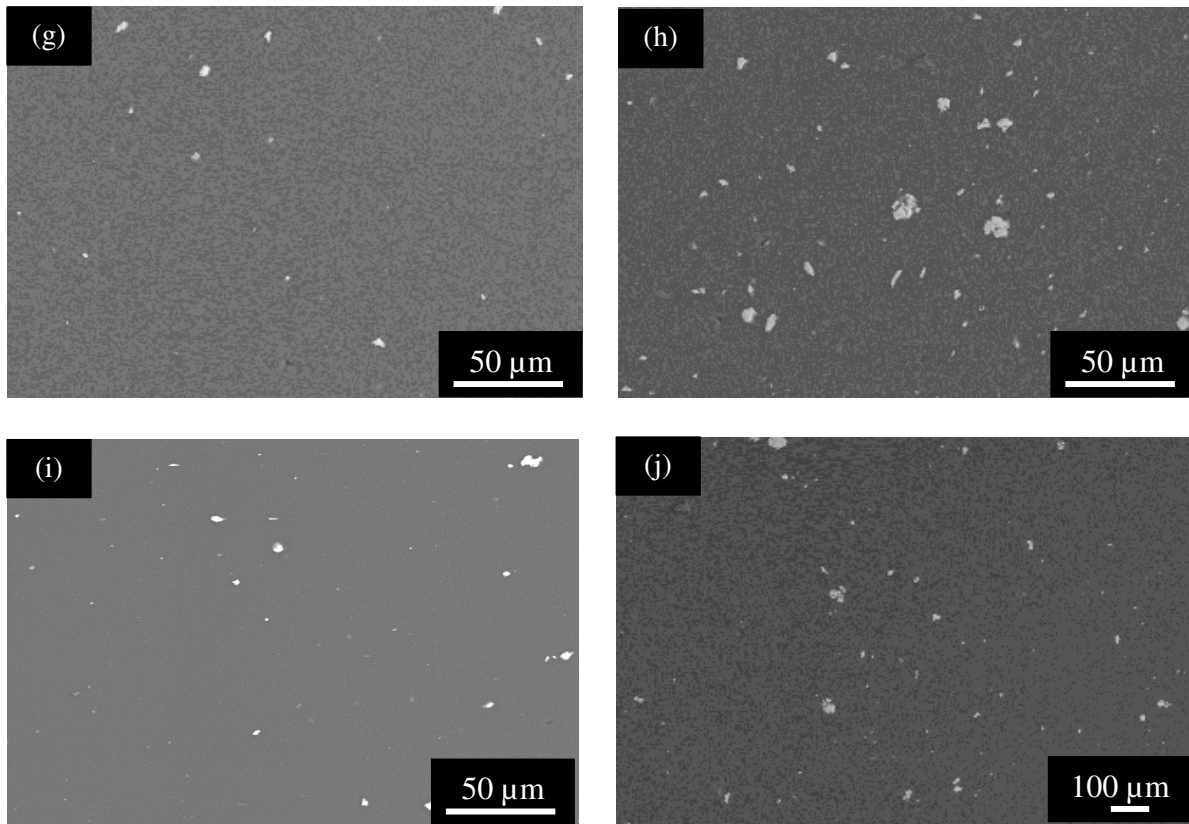


Figure 3.5: SEM micrographs of 3D printed, (a) PLA in SE,, and BSE images of, (b) BSE of (a), (c) PLA-1wt% MoAlB, (d) PLA-5wt% MoAlB, (e) PLA-1wt%  $Ti_3SiC_2$ , (f) PLA-5wt%  $Ti_3SiC_2$ , (g) PLA-1wt%  $Ti_3AlC_2$ , (h) PLA-5wt% $Ti_3AlC_2$ , (i) PLA-1wt% $Cr_2AlC$ , and (j) PLA-5wt% $Cr_2AlC$ .

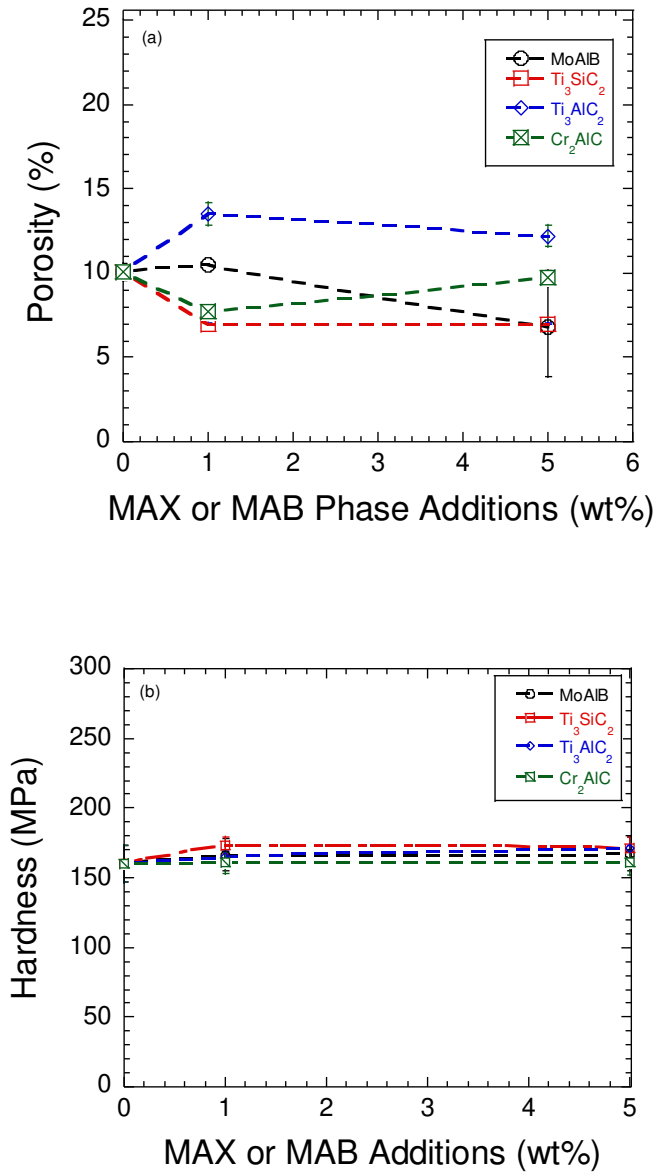
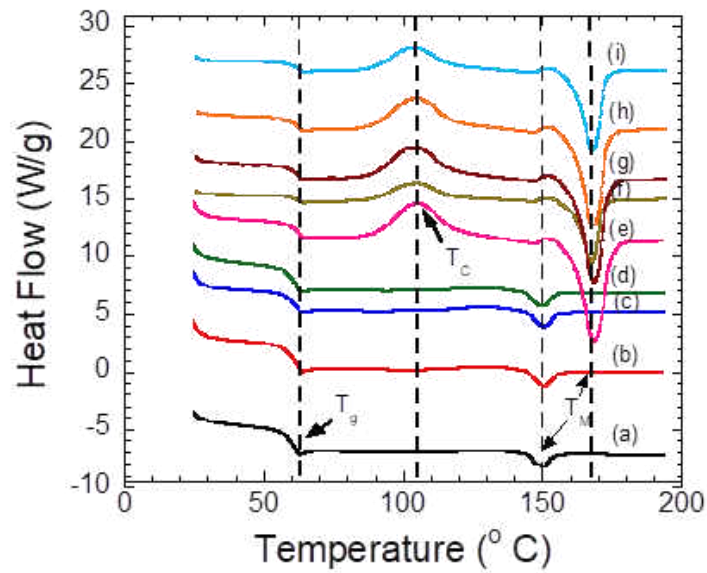


Figure 3.6: Plot of, (a) porosity, and (b) hardness versus MAX or MAB content in the PLA matrix.



3.7: DSC analysis of, (a) PLA, (b) PLA-1 wt% MoAlB, (c) PLA-5 wt% MoAlB, (d) PLA-1wt% Ti<sub>3</sub>SiC<sub>2</sub>, (e) PLA-5 wt% Ti<sub>3</sub>SiC<sub>2</sub>, (f) PLA-1 wt% Ti<sub>3</sub>AlC<sub>2</sub>, (g) PLA-5 wt% Ti<sub>3</sub>AlC<sub>2</sub>, (h) PLA-1 wt% Cr<sub>2</sub>AlC, and (i) PLA-5 wt% Cr<sub>2</sub>AlC.

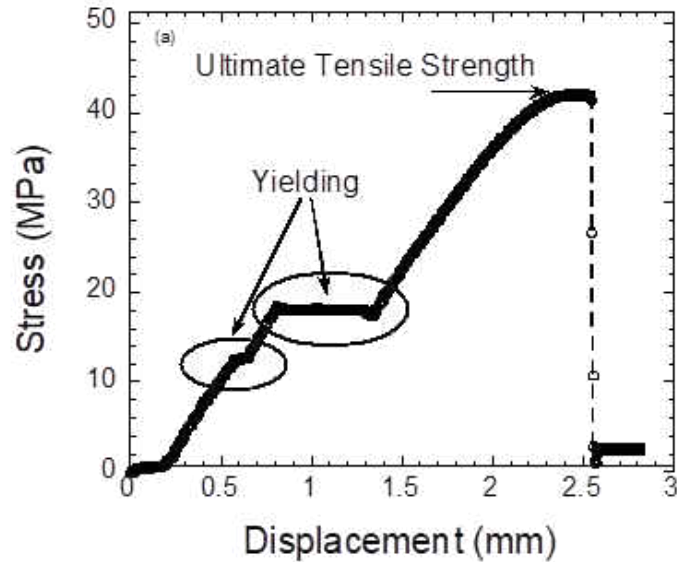


Figure 3.8: Plot of tensile stress versus displacement of 3D printed PLA.



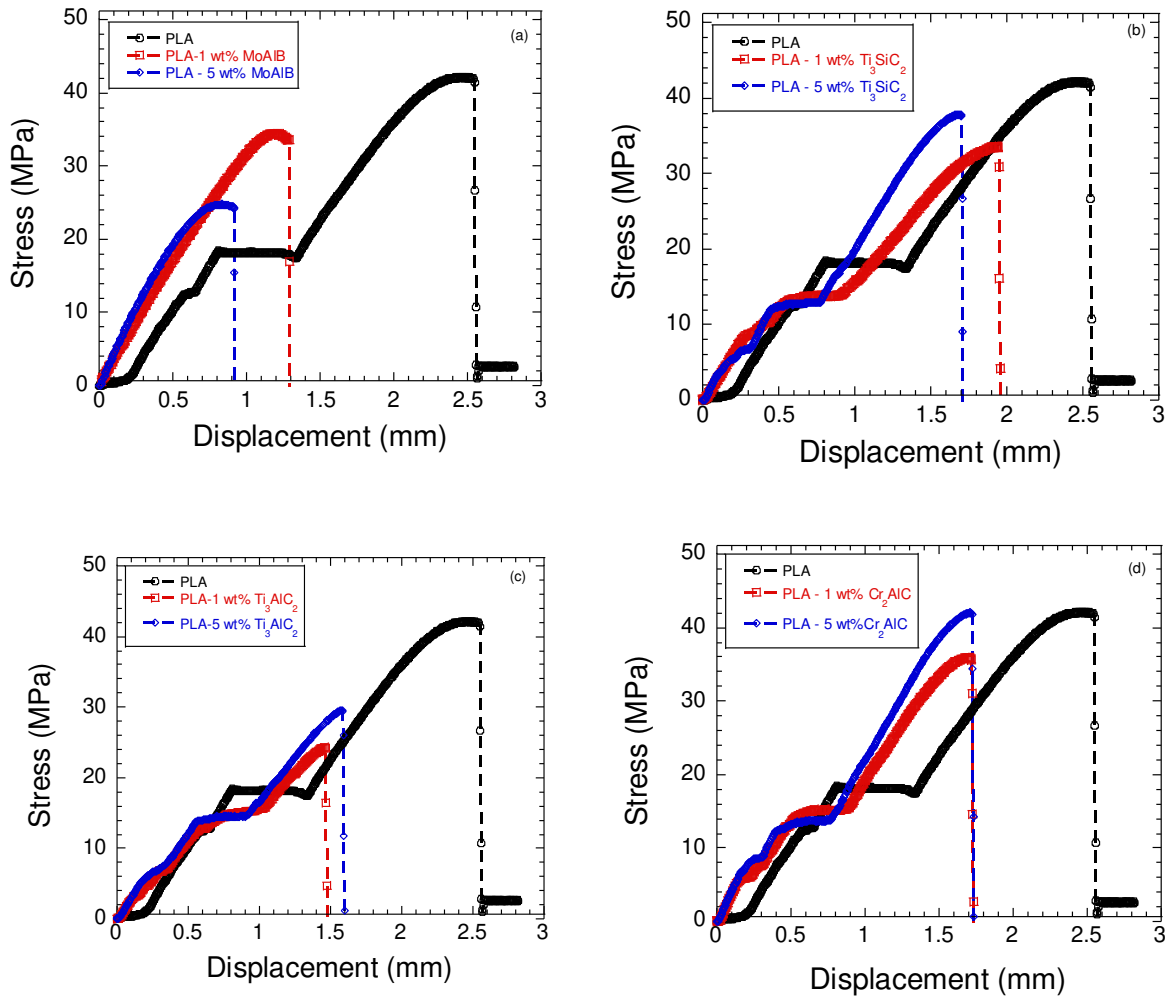


Figure 3.9: Plot of tensile stress versus displacement of, (a) PLA-MoAlB, (b) PLA-Ti<sub>3</sub>SiC<sub>2</sub>, (c) PLA-Ti<sub>3</sub>AlC<sub>2</sub>, and (d) PLA-Cr<sub>2</sub>AlC.

Figure 3.9 shows the tensile stress versus displacement plot of different PLA based composites. In general, all the compositions failed at lower strength than PLA. Figure 3.10 summarizes the UTS as function of MAX or MoAlB concentration. All the compositions showed a drop in UTS after the addition of 1 wt% MAX or MoAlB which corresponds 0.2-0.3 vol% of these phases (Table 3.1). Based on these results, we can conclude that PLA matrix is sensitive to these phases and can affect the mechanical behavior of these composites. Interestingly, the addition

of 5 wt% MAX phases improved the UTS of these composites, for example, PLA-5wt%Ti<sub>3</sub>SiC<sub>2</sub>, PLA-5wt%Ti<sub>3</sub>AlC<sub>2</sub> and PLA-5wt%Cr<sub>2</sub>AlC had a UTS of ~39 MPa, ~30.5 MPa, and ~38.7 MPa as compared to ~41.5 MPa in pure PLA. Comparatively, PLA-5wt%MoAlB had a UTS of ~23.2 MPa. By analyzing these results, it can be summarized that certain crystalline PLA-MAX composites like PLA-Ti<sub>3</sub>SiC<sub>2</sub> and PLA-Cr<sub>2</sub>AlC have higher strength as compared to PLA-Ti<sub>3</sub>AlC<sub>2</sub>. Comparatively, amorphous PLA-MoAlB composites were not able to recover their strength. Detailed studies are recommended for correlating the effect of, (a) higher volume fractions, (b) crystallization, and (c) crystal chemistry on the mechanical strength of these novel composites.

Figure 3.11 shows the variation of  $\mu_{\text{mean}}$  and WR as function of MAX phases or MoAlB content. PLA had  $\mu_{\text{mean}}$  and WR of  $0.34 \pm 0.04$  and  $7.7 \times 10^{-5} \text{ mm}^3/\text{Nm}$ , respectively. In all cases,  $\mu_{\text{mean}}$  decreased by ~76% of  $\mu_{\text{mean}}$  in PLA after the addition of 1 wt% particulates to ~0.27, ~0.26, ~0.26, and ~0.26 in PLA-1wt%MoAlB, PLA-1wt%Ti<sub>3</sub>SiC<sub>2</sub>, PLA-1wt%Ti<sub>3</sub>AlC<sub>2</sub>, and PLA-1wt%Cr<sub>2</sub>AlC, respectively. It retained similar value in all the compositions after the addition of 5 wt% particulates except PLA-5wt%Ti<sub>3</sub>AlC<sub>2</sub> where it increased marginally to ~0.30. The WR marginally decreased in PLA-1wt%Cr<sub>2</sub>AlC to  $\sim 2.2 \times 10^{-5} \text{ mm}^3/\text{Nm}$  or retained similar values of  $7.72 \times 10^{-5} \text{ mm}^3/\text{Nm}$  and  $5.28 \times 10^{-5} \text{ mm}^3/\text{Nm}$  in PLA-1wt%MoAlB and PLA-1wt%Ti<sub>3</sub>AlC<sub>2</sub>, respectively, and increased to  $\sim 1.6 \times 10^{-4} \text{ mm}^3/\text{Nm}$  in PLA-1wt%Ti<sub>3</sub>SiC<sub>2</sub>. After the addition of 5 wt% particulates, the WR of all compositions increased to  $\sim 3 \times 10^{-4} \text{ mm}^3/\text{Nm}$ ,  $\sim 1.4 \times 10^{-4} \text{ mm}^3/\text{Nm}$ , and  $\sim 1.8 \times 10^{-4} \text{ mm}^3/\text{Nm}$  in PLA-5wt%MoAlB, PLA-5wt%Ti<sub>3</sub>SiC<sub>2</sub>, and PLA-5wt%Ti<sub>3</sub>AlC<sub>2</sub>, respectively except PLA-5wt%Cr<sub>2</sub>AlC where it retained similar value of  $\sim 8.3 \times 10^{-5} \text{ mm}^3/\text{Nm}$ , respectively. By inspecting the data, it can be surmised that Cr<sub>2</sub>AlC is performing better as a solid lubricant as compared to the other phases. Figures 3.12 a-b show the tribosurfaces of PLA (Fig. 3.12a), and the corresponding stainless-steel surface (Fig. 3.12b). Ligaments of PLA fragments

can be observed on the stainless-steel surface. Similarly, Figs. 3.12 c-d show tribosurfaces of PLA-5wt%Cr<sub>2</sub>AlC and the corresponding stainless-steel surface. Wear track was observed on the PLA-5wt%Cr<sub>2</sub>AlC surface (Fig. 3.12c). Ligaments of polymers wear debris was observed on the stainless surface (Fig. 3.12e). On further investigation, polymer wear debris reinforced with partially oxidized Cr<sub>2</sub>AlC particulates was observed (Fig. 3.12f). These micrographs give further evidence that Cr<sub>2</sub>AlC particles are effective solid lubricants by intermingling with the base polymer and proving a robust interfacial layer which decreased  $\mu_{\text{mean}}$  without compromising the WR. In future, it would be interesting to study etching or other mechanical treatments to increase the attachment of interfacial layers to the substrates. At this juncture, it is also not clear why Cr<sub>2</sub>AlC is behaving better than the other systems which were testing during this study. More studies are needed to understand the effect of MAX or MoAlB on the interfacial layers.

Figure 3.13 shows the wettability profile of all the composites. PLA and all the 3D printed composites were hydrophilic (Fig. 3.14).

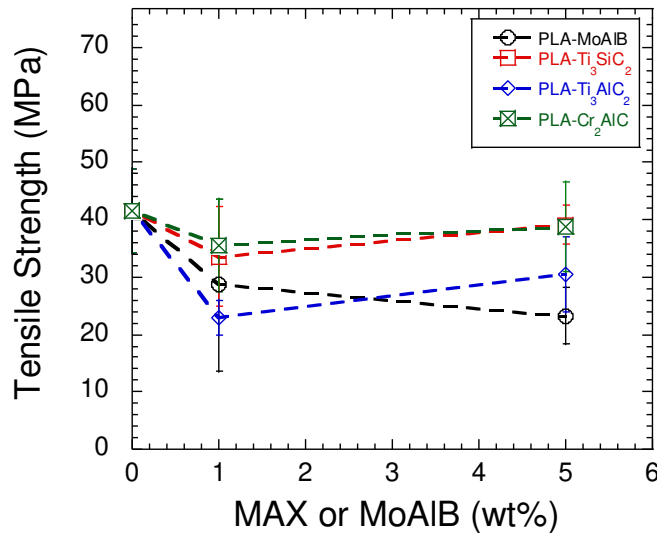


Figure 3.10: Plot of tensile strength versus MAX or MoAlB additions in the PLA matrix.

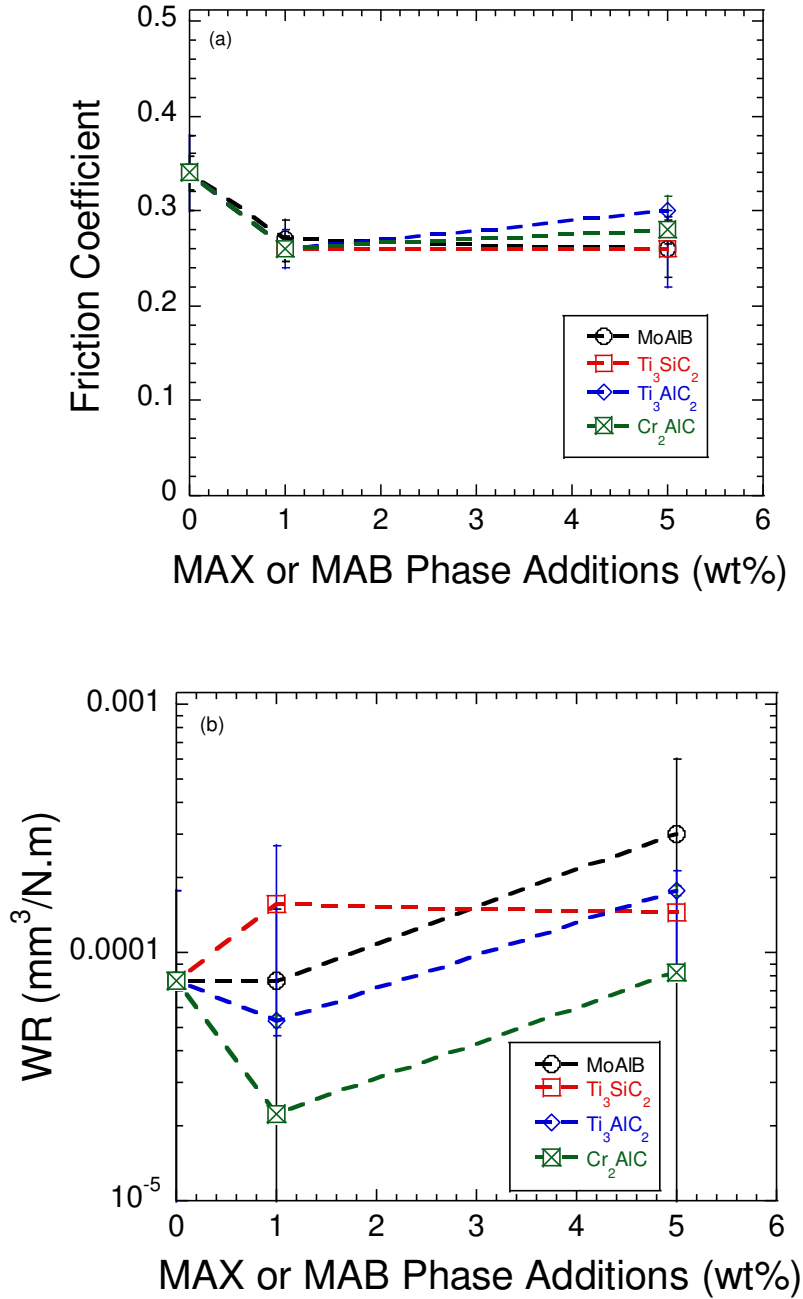


Figure 3.11: Plot of, (a) friction coefficient, and (b) WR versus MAX or MAB additions in PLA matrix.

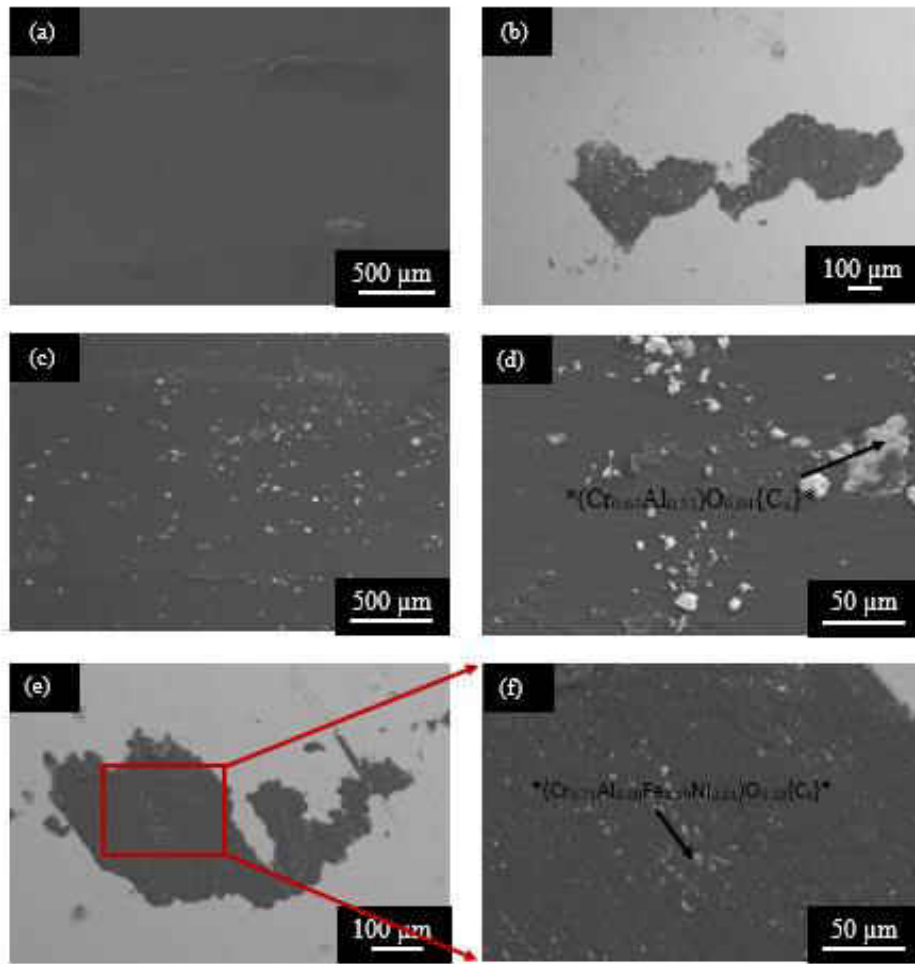


Figure 3.12: SEM micrographs of, (a) PLA in SE, (b) BSE image of the 100 Cr6 Stainless steel surface, (c) PLA-5wt%Cr<sub>2</sub>AlC in BSE, (d) higher magnification of PLA-5wt%Cr<sub>2</sub>AlC in BSE, (e) Stainless steel surface in BSE, and (f) BSE of the region marked in (e) after tribological testing.

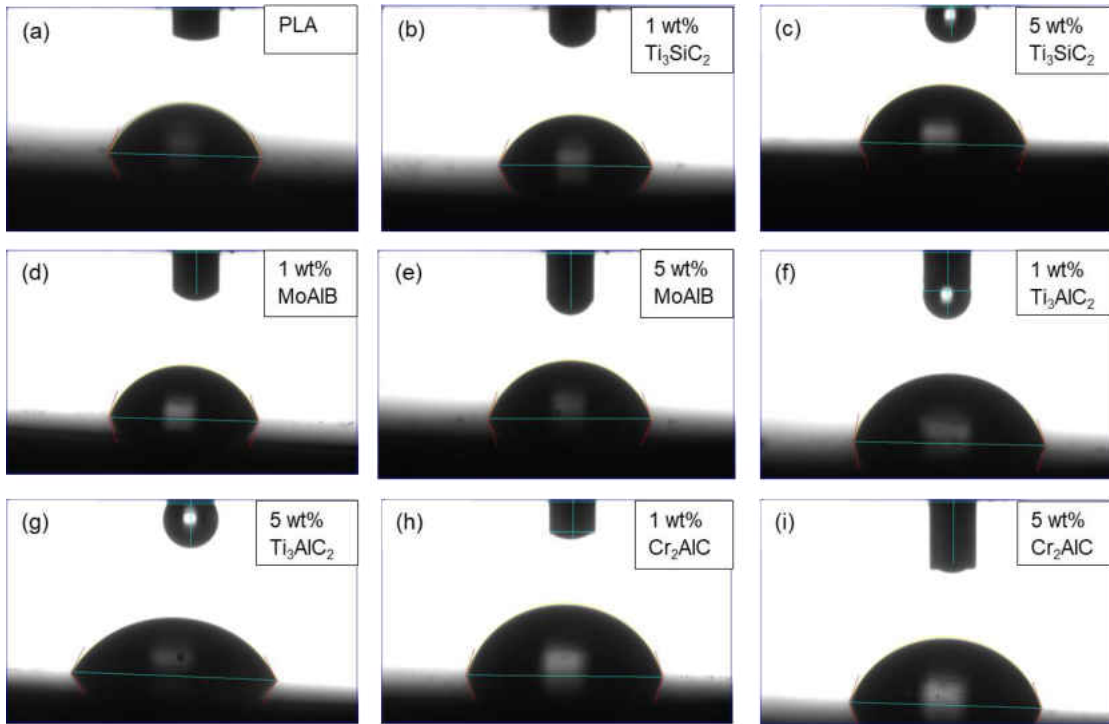


Figure 3.13: Wettability profile of, (a) PLA, (b) PLA-1wt% $Ti_3SiC_2$ , (c) PLA-5wt% $Ti_3SiC_2$ , (d) PLA-1wt%MoAlB, (e) PLA-5 wt% MoAlB, (f) PLA-1wt%  $Ti_3AlC_2$ , (g) PLA-5wt%  $Ti_3AlC_2$ , (h) PLA-1 wt%  $Cr_2AlC$ , and (i) PLA-5 wt% $Cr_2AlC$ .

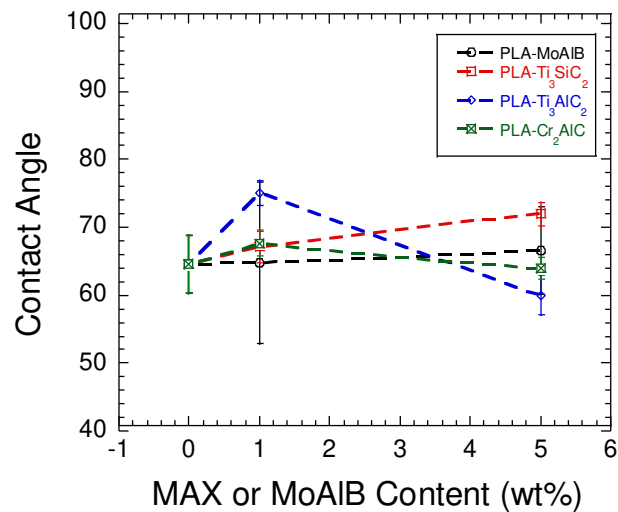


Figure 3.14: Plot of contact angle as a function of MAX or MoAlB content.

### 3.4 Conclusions

MAX-reinforced polymer matrix composites were successfully designed by 3D printing. From the results, it can be concluded that MAX Phases changed the crystallinity of the base PLA matrix and increased the melting temperature to  $\sim 170$  °C from  $\sim 150$  °C in the base PLA composition. More studies are needed to understand the exact mechanisms of crystallization in the PLA matrix by using MAX phases. The MAX Phase powders acted as a solid lubricant by decreasing the friction coefficient for all cases. In addition, it was also observed that the addition of 1 wt% decreased the WR for all compositions except  $\text{Ti}_3\text{SiC}_2$  but the WR then increased at 5 wt% additions for all the compositions except  $\text{Cr}_2\text{AlC}$ .

## CHAPTER IV

### CONCLUSIONS AND FUTURE WORK

#### 4.1 Future Studies on Lignin-PLA Composites

It is highly recommended that PLA-Lignin composites should be made with Fused Deposition Modelling (FDM). Preliminary studies showed that it is tedious to incorporate as-received lignin in the PLA matrix

#### 4.2 Experimental

As-received lignin powder was added to the PLA polymer matrix in 1 and 5 wt% compositions. This was done by mixing the two powders (lignin and pulverized PLA) in a polymethyl methacrylate (PMMA) mixing container with 3 PMMA mixing balls for 5 minutes. The powders were then extruded from the extruder (Filabot EX2 Extruder, Filabot, Barre, VT). Attempts to extrude this mixture into uniform filament were unsuccessful due to bubble formation in the filament. Even after systematic efforts to troubleshoot the problem by adjusting temperature by 5°C increments until 155°C but it did not ameliorate the situations, and the bubbling in the filaments persisted. We focused on addressing the problem by heat treating lignin at different temperatures.

Currently, we are exploring heat treatment of the lignin powder. Initially, lignin was heat treated at 300°C for 1 hour in an Ar atmosphere. The heat-treated lignin was then crushed to a fine powder using a SS container and two SS balls in a ball mill for 10 minutes. The fine powder was



then sieved for 1 hour into -325 mesh. The -325 mesh fraction was used for mixing with the pulverized PLA powder. Thereafter, 1 and 5 wt% of these powders were then mixed with PLA by using the method described in the previous paragraph. The heat-treated lignin-PLA powder mixture was extruded from the extruder at 170°C. Currently, dog-bone and cylindrical samples of the same dimensions as the MAXPOL test coupons were printed with the Afinia H400 3D printer. The samples printed have yet to be tested.

#### 4.3 Concluding Remarks

Heat treatment of the lignin aided in the incorporation of lignin to the PLA polymer matrix. Extrusion of heat-treated lignin and PLA mixture was successful, and the filament produced was successfully printed into test coupons. It is also planned to heat treat the lignin powders to 500°C, 700°C, and 900°C to determine the effect of heat treatment on the 3D printed composites.

## APPENDIX

### References

- [1] Numata, K., and D.I. Kaplan. “Biologically Derived Scaffolds.” *Advanced Wound Repair Therapies*, 2011, pp. 524–551., doi:10.1533/9780857093301.4.524.
- [2] Shankar, Shiv, and Jong-Whan Rhim. “Bionanocomposite Films for Food Packaging Applications.” *Reference Module in Food Science*, 2018, pp. 1–10., doi:10.1016/b978-0-08-100596-5.21875-1.
- [3] Jamshidian, Majid, et al. “Poly-Lactic Acid: Production, Applications, Nanocomposites, and Release Studies.” *Comprehensive Reviews in Food Science and Food Safety*, vol. 9, no. 5, 2010, pp. 552–571., doi:10.1111/j.1541-4337.2010.00126.x.
- [4] Mohan, Sneha, et al. “Biopolymers – Application in Nanoscience and Nanotechnology.” *Recent Advances in Biopolymers*, 2016, doi:10.5772/62225.
- [5] Chen, H. “Chemical Composition and Structure of Natural Lignocellulose.” *Biotechnology of Lignocellulose Theory and Practice*, Springer Netherlands, 2014, pp. 25–26, 47–54. doi.org/10.1007/978-94-007-6898-7\_2
- [6] Dart, R. K., Betts W.B. “Uses and Potential of Lignocellulose .” *Biodegradation: Natural and Synthetic Materials*, Springer Series in Applied Biology, Springer, London, 1991, pp. 201–202.
- [7] Christopher, Lew Paul, Bin Yao, and Yun Ji “Lignin Biodegradation with Laccase-Mediator Systems.” *Frontiers in Energy Research*, vol. 2, 2014., doi.org/10.3389/fenrg.2014.00012
- [8] Tolbert, Allison, et al. “Characterization and Analysis of the Molecular Weight of Lignin for Biorefining Studies.” *Biofuels, Bioproducts and Biorefining*, vol. 8, no. 6, 2014, pp. 836–856., doi:10.1002/bbb.1500.
- [9] Bozell, J. J., Holladay, J. E., Johnson, D., and White, J. F. (2007). “Top Value Added Candidates from Biomass, Volume II: Results of Screening for Potential Candidates from Biorefinery Lignin”. Richland, WA: Pacific Northwest National Laboratory.
- [10] Thielemans, Wim, and Richard P. Wool. “Lignin Esters for Use in Unsaturated Thermosets: Lignin Modification and Solubility Modeling.” *Biomacromolecules*, vol. 6, no. 4, 2005, pp. 1895–1905., doi:10.1021/bm0500345.

- [11] Duval, Antoine, and Martin Lawoko. "A Review on Lignin-Based Polymeric, Micro- and Nano-Structured Materials." *Reactive and Functional Polymers*, vol. 85, 2014, pp. 78–96., doi:10.1016/j.reactfunctpolym.2014.09.017.
- [12] Jeong, Heonyoung, et al. "Use of Acetylated Softwood Kraft Lignin as Filler in Synthetic Polymers." *Fibers and Polymers*, vol. 13, no. 10, 2012, pp. 1310–1318., doi:10.1007/s12221-012-1310-6.
- [13] Krall, Eric M., et al. "Catalyst-Free Lignin Valorization by Acetoacetylation. Structural Elucidation by Comparison with Model Compounds." *Green Chemistry*, vol. 20, no. 13, 2018, pp. 2959–2966., doi:10.1039/c8gc01071d.
- [14] Shweta, Kumari, and Harit Jha. "Rice Husk Extracted Lignin–TEOS Biocomposites: Effects of Acetylation and Silane Surface Treatments for Application in Nickel Removal." *Biotechnology Reports*, vol. 7, 2015, pp. 95–106., doi:10.1016/j.btre.2015.05.003.
- [15] Agarwal, Ashutosh, et al. "Advancement in Technologies for the Depolymerization of Lignin." *Fuel Processing Technology*, vol. 181, 2018, pp. 115–132., doi:10.1016/j.fuproc.2018.09.017.
- [16] Spiridon, Iuliana, et al. "Evaluation of PLA–Lignin Bioplastics Properties before and after Accelerated Weathering." *Composites Part B: Engineering*, vol. 69, 2015, pp. 342–349., doi:10.1016/j.compositesb.2014.10.006.
- [17] Gupta, S., M.F. Riyad, and Yun Ji. "Synthesis and Tribological Behavior of Ultra High Molecular Weight Polyethylene (UHMWPE)-Lignin Composites." *Lubricants*, vol. 4, no. 3, 2016, p. 31., doi:10.3390/lubricants4030031.
- [18] Flynt, Joseph. "Polylactic Acid (PLA): The Environment-Friendly Plastic." *3D Insider*, 9 Nov. 2017.[Online] Available: <https://3dinsider.com/what-is-pla/>, Accessed December 5,2018
- [19] Ameen, Sara M. and Giorgia Caruso "Chemistry of Lactic Acid." *Lactic Acid in the Food Industry*, SpringerBriefs in Molecular Science, Springer Cham, 2017, pp. 7–15. doi.org/10.1007/978-3-319-58146-0\_2
- [20] Farah, Shady, et al. "Physical and Mechanical Properties of PLA, and Their Functions in Widespread Applications - A Comprehensive Review." *Advanced Drug Delivery Reviews*, vol. 107, 2016, pp. 367–392., doi:10.1016/j.addr.2016.06.012.
- [21] Kamthai, Suthaphat, and Rathanawan Magaraphan. "Thermal and Mechanical Properties of Polylactic Acid (PLA) and Bagasse Carboxymethyl Cellulose (CMCB) Composite by Adding Isosorbide Diesters." *AIP Conference Proceedings* 1664, 060006, 2015, doi: 10.1063/1.4918424
- [22] Sujaritjun, Wassamon, et al. "Mechanical Property of Surface Modified Natural Fiber Reinforced PLA Biocomposites." *Energy Procedia*, vol. 34, 2013, pp. 664–672. doi.org/10.1016/j.egypro.2013.06.798

- [23] Tian, Xiaoyong, et al. "Recycling and Remanufacturing of 3D Printed Continuous Carbon Fiber Reinforced PLA Composites." *Journal of Cleaner Production*, vol. 142, 2017, pp. 1609–1618., doi:10.1016/j.jclepro.2016.11.139.
- [24] Scaffaro, Roberto, et al. "PLA Based Biocomposites Reinforced with Posidonia Oceanica Leaves." *Composites Part B: Engineering*, vol. 139, 2018, pp. 1–11., doi:10.1016/j.compositesb.2017.11.048.
- [25] Barsoum, M. W. "MAX Phases: Properties of Machinable Ternary Carbides and Nitrides." Wiley-VCH Verlag GmbH & Co. KGaA, 2013.
- [26] Radovic, Miladin, and Michel W. Barsoum. "MAX Phases: Bridging the Gap between Metals and Ceramics." *American Ceramic Society Bulletin*, vol. 92, no. 3, 2013.
- [27] M.W. Barsoum and T. El-Raghy, "The MAX Phases: Unique New Carbide and Nitride Materials", *American Scientist*, 89, 334-343 (2001)., doi:10.1511/2001.28.736.
- [28] Md. Atikur Rahman, Md. Zahidur Rahaman. "Study on Structural, Electronic, Optical and Mechanical Properties of MAX Phase Compounds and Applications Review Article." *American Journal of Modern Physics*. Vol. 4, No. 2, 2015, pp. 75-91. doi: 10.11648/j.ajmp.20150402.15
- [29] Eklund, Per, et al. "The Mn+1AX<sub>n</sub> Phases: Materials Science and Thin-Film Processing." *Thin Solid Films*, vol. 518, no. 8, 2010, pp. 1851–1878., doi:10.1016/j.tsf.2009.07.184.
- [30] Xu, Ludi, et al. "Synthesis, Microstructure and Properties of MoAlB Ceramics." *Ceramics International*, vol. 44, no. 11, 2018, pp. 13396–13401., doi:10.1016/j.ceramint.2018.04.177.
- [31] Kota, Sankalp, et al. "Synthesis and Characterization of an Alumina Forming Nanolaminated Boride: MoAlB." *Scientific Reports*, vol. 6, no. 26475, 2016, pp. 1–9., doi:10.1038/srep26475.
- [32] Benamor, Abdessabour, et al. "Friction and Wear Properties of MoAlB against Al<sub>2</sub>O<sub>3</sub> and 100Cr6 Steel Counterparts." *Journal of the European Ceramic Society*, 2018. DOI:10.1016/j.jeurceramsoc.2018.10.026.
- [33] "What Is Additive Manufacturing?" *GE Additive*, General Electric, 2018. [Online]. Available: <https://www.ge.com/additive/additive-manufacturing>. Accessed December 5, 2018.
- [34] "Introduction to FDM 3D Printing." *3D Hubs*, 3D Hubs Blog, 2018. [Online] Available: <https://www.3dhubs.com/knowledge-base/introduction-fdm-3d-printing>, Accessed December 5, 2018
- [35] "Fused Deposition Modeling (FDM)." *GE Additive*, General Electric, 2018. [Online] Available: <https://www.ge.com/additive/additive-manufacturing/information/fused-deposition-modeling-technology>. Accessed December 5, 2018

- [36] “About Additive Manufacturing: Material Jetting.” *Additive Manufacturing Research Group*, Loughborough University, 2018. [Online] Available: <https://www.lboro.ac.uk/research/amrg/about/the7categoriesofadditivemanufacturing/materialjetting/>. Accessed December 5, 2018
- [37] “Engine SR.” *Hyrel 3D*, 2018. [Online] Available: <http://www.hyrel3d.com/>, Accessed December 5, 2018
- [38] Gupta, S., and M. Fuka. “Synthesis of MoAlB Particulates and Their Porous Derivatives by Selective Deintercalation of Al from MoAlB.” *Energy Technology 2018 The Minerals, Metals & Materials Series*, 2018, pp. 535–541., doi:10.1007/978-3-319-72362-4\_50.
- [39] Fuka, Matt, et al. “Design and Synthesis of Novel Nano-Laminated Particulates for Fabricating Novel Multifunctional Composites.” *International Journal of Innovative Research in Science, Engineering and Technology*, vol. 5, no. 12, Dec. 2016, pp. 20936–20940. DOI:10.15680/IJIRSET.2016.0512138
- [40] Dey, Maharshi. “Synthesis and Characterization of Novel Ni-MAX and AlSi-MAX Composites.” University of North Dakota, ProQuest LLC, 2018.
- [41] Filabot, 2018 [Online] Available: <https://www.filabot.com/>, Accessed December 5, 2018.
- [42] “Afinia H400 3D Printer” *Afinia 3D*, 2018. [Online] Available: <http://afinia.com/3d-printers/h400/>, Accessed December 5, 2018.
- [43] Dunnigan, R., et al. “Beneficial Usage of Recycled Polymer Particulates for Designing Novel 3D Printed Composites.” *Progress in Additive Manufacturing*, vol. 3, no. 1-2, 2018, pp. 33–38. doi.org/10.1007/s40964-018-0046-2.
- [44] B. Bindhu, R. Renisha, Libin Roberts, and T.O. Varghese, “Boron Nitride reinforced polylactic acid composites film for packaging: Preparation and properties”, *Polymer Testing* 66 (2018) 172–177.
- [45] Adrián Rodríguez-Panes, Juan Claver and Ana María Camacho, “The Influence of Manufacturing Parameters on the Mechanical Behaviour of PLA and ABS Pieces Manufactured by FDM: A Comparative Analysis”, *Materials* 2018, 11, 1333; doi:10.3390/ma11081333.